



This is a repository copy of *Late Pleistocene-Holocene alluvial stratigraphy of southern Baja California, Mexico*.

White Rose Research Online URL for this paper:
<http://eprints.whiterose.ac.uk/160048/>

Version: Accepted Version

Article:

Antinao, J.L., McDonald, E., Rhodes, E.J. orcid.org/0000-0002-0361-8637 et al. (4 more authors) (2016) Late Pleistocene-Holocene alluvial stratigraphy of southern Baja California, Mexico. *Quaternary Science Reviews*, 146. pp. 161-181. ISSN 0277-3791

<https://doi.org/10.1016/j.quascirev.2016.06.008>

Article available under the terms of the CC-BY-NC-ND licence
(<https://creativecommons.org/licenses/by-nc-nd/4.0/>).

Reuse

This article is distributed under the terms of the Creative Commons Attribution-NonCommercial-NoDerivs (CC BY-NC-ND) licence. This licence only allows you to download this work and share it with others as long as you credit the authors, but you can't change the article in any way or use it commercially. More information and the full terms of the licence here: <https://creativecommons.org/licenses/>

Takedown

If you consider content in White Rose Research Online to be in breach of UK law, please notify us by emailing eprints@whiterose.ac.uk including the URL of the record and the reason for the withdrawal request.



eprints@whiterose.ac.uk
<https://eprints.whiterose.ac.uk/>

1 **Late Pleistocene-Holocene alluvial stratigraphy of southern Baja California, Mexico.**

2

3 José Luis Antinao (*)^{1,2}

4 Eric McDonald ¹

5 Edward J. Rhodes,^{3,4} Nathan Brown³, Wendy Barrera³

6 John C. Gosse ⁵

7 Susan Zimmermann ⁶

8

9 ¹ Division of Earth and Ecosystem Sciences, Desert Research Institute, 2215 Raggio Parkway
10 Reno NV 89512, USA.

11 ² National Research Center for Integrated Natural Disaster Management, CIGIDEN, Santiago
12 7820436, Chile

13 ³ Earth and Space Sciences Department, UCLA, Los Angeles, CA90095, USA.

14 ⁴ Department of Geography, University of Sheffield, Western Bank, Sheffield, S10 2TN, UK.

15 ⁵ Dalhousie Geochronology Centre, Dalhousie University, Halifax, Nova Scotia, Canada
16 B3H4J1.

17 ⁶Center for Accelerator Mass Spectrometry, Lawrence Livermore National Laboratory,
18 CA94550, USA.

19 (*) Corresponding author: +1 (775) 673 7450.

20

21 Abstract

22 A late Pleistocene to Holocene alluvial stratigraphy has been established for the basins of La Paz
23 and San José del Cabo, in the southern tip of the Baja California peninsula, Mexico. Six discrete
24 alluvial units (Qt1 through Qt6) were differentiated across the region using a combination of
25 geomorphologic mapping, sedimentological analysis, and soil development. These criteria were
26 supported using radiocarbon, optically stimulated luminescence and cosmogenic depth-profile
27 geochronology. Major aggradation started shortly after ~70 ka (Qt2), and buildup of the main
28 depositional units ended at ~10 ka (Qt4). After deposition of Qt4, increasing regional incision of
29 older units and the progressive development of a channelized alluvial landscape coincide with
30 deposition of Qt5 and Qt6 units in a second, incisional phase. All units consist of multiple 1-3 m
31 thick alluvial packages deposited as upper-flow stage beds that represent individual storms. Main

32 aggradational units (Qt2-Qt4) occurred across broad (>2 km) channels in the form of sheetflood
33 deposition while incisional stage deposits are confined to channels of ~0.5-2 km width.
34 Continuous deposition inside the thicker (>10 m) pre-Qt5 units is demonstrated by closely
35 spaced dates in vertical profiles. In a few places, disconformities between these major units are
36 nevertheless evident and indicated by partly eroded buried soils. The described units feature
37 sedimentological traits similar to historical deposits formed by large tropical cyclone events, but
38 also include characteristics of upper-regime flow sedimentation not shown by historical
39 sediments, like long (>10 m) wavelength antidunes and transverse ribs. We interpret the whole
40 sequence as indicating discrete periods during the late Pleistocene and Holocene when climatic
41 conditions allowed larger and more frequent tropical cyclone events than those observed
42 historically. These discrete periods are associated with times when insolation at the tropics was
43 higher than the present-day conditions, determined by precessional cycles, and modulated by the
44 presence of El Niño-like conditions along the tropical and northeastern Pacific. The southern
45 Baja California alluvial record is the first to document a precession-driven alluvial chronology
46 for the region, and it constitutes a strong benchmark for discrimination of direct tropical
47 influence on any other alluvial record in southwestern North America.

48

49 1. Introduction

50 In southwestern North America, dry periods alternated with periods of enhanced effective
51 moisture relative to present-day conditions during the late Quaternary (e.g., Li et al., 2008; Kirby
52 et al., 2013; Roy et al., 2013). Knowledge regarding paleoclimate conditions for this region is
53 primarily derived from the analysis of records from lacustrine sediments, marine cores, and
54 speleothems (Kirby et al., 2012, 2013; Wagner et al., 2010). Alluvial environments are also
55 critical indicators of environmental change related to time-transgressive changes in climate (cf.
56 Bull, 1991). Changes in sediment yield and the timing of regional fluvial aggradation are
57 particularly sensitive to factors such as extreme runoff events and as such can give indications of
58 the hydroclimatological state of a region (cf. Parker, 1995; Huckleberry, 1996; Etheredge et al.,
59 2004; Webb et al., 2008). Extracting paleoclimate histories from alluvial records has been
60 limited, however, because of the difficulties in establishing a well-dated chronological
61 framework for alluvial deposits, as discussed in e.g. Mahan et al. (2007), Miller et al. (2010), and
62 Owen et al. (2014).

63 We introduce here a well-dated record for alluvial deposition in the southern portion of
64 the Baja California peninsula, in Northwestern Mexico (Fig. 1). The region has experienced
65 steady Quaternary tectonic activity (cf. Umhoefer et al., 2014; Busch et al., 2011) that has
66 allowed the generation of accommodation space thus favoring the preservation of sediment
67 deposits over time. The area also is a sensitive environment for recording climate oscillations
68 arising from direct tropical influence, outside of the present-day reach of the mid-latitude winter
69 cyclone storm tracks (Fig. 1). The region is also located in a marginal area respect to the core
70 region of the North American Monsoon (Englehardt and Douglas, 2001; Gutzler, 2004; Diaz et
71 al., 2008; Arriaga-Ramirez and Cavazos, 2010). Tropical cyclones affect the southern peninsula
72 at least once or twice per year (e.g., Farfán, 2004; Farfán and Fogel, 2007); major intense
73 tropical cyclones affect the area once every three to six years (e.g., Villanueva, 2001; Antinao
74 and McDonald, 2011). These major tropical storms bring extensive geomorphic impacts
75 associated with fan delta progradation along the coast, alluvial channel erosion and
76 sedimentation (Martínez-Gutiérrez and Mayer, 2004), and erosion in hillslopes, with pervasive
77 rilling and landsliding (Antinao and Farfán, 2013). These impacts are much larger than any of
78 those observed for storms affecting the southern peninsula either as mesoscale convective
79 systems associated with the NAM (without tropical storm influence) or during the winter (frontal
80 storms) as documented e.g., in Villanueva (2001), Martínez-Gutiérrez and Mayer (2004), and
81 Antinao and McDonald (2011).

82 The benchmark chronology presented here is aimed to understand alluvial deposition and
83 incision in this region, and it is a valuable tie between tropical variability and environmental
84 changes in arid southwestern North America. The morphogenetic sequence introduced here can
85 also be used for comparison and interpretation of paleoenvironmental data for nearby areas in
86 northwestern Mexico and southwest USA. The objectives of this paper are: (1) to describe the
87 morphostratigraphic sequence of accumulated alluvial deposits developed from
88 geomorphological, sedimentological and pedogenetic evidences and supported by radiocarbon,
89 luminescence and cosmogenic dating; (2) to provide an interpretation of its paleoenvironmental
90 significance, and (3) to analyze the alluvial sequence in the context of climate variation recorded
91 globally and regionally for southwestern North America, providing a dynamic explanation for
92 the evolution of alluvial aggradation during the last 70,000 years.

93

94 2. Study area

95 Southern Baja California has experienced moderate tectonic uplift developed in response
96 to rifting since 12 Ma along the Pacific-North American Plate margin (e.g., Fletcher and
97 Munguía, 2000) with relief generation and opening of related basins. The most prominent
98 alluvial basins are La Paz, San Juan, and San José del Cabo (Fig. 1). The basins have been filled
99 by a succession of marine and continental sediments (Martínez-Gutierrez and Sethi, 1997;
100 Fierstine et al., 2001; Busch et al., 2011). Quaternary sediments of the continental El Chorro
101 Formation (Martínez-Gutierrez and Sethi, 1997) top the sedimentary fill, deposited in alluvial
102 fans that radiate from the Sierra La Laguna, northwest of San José del Cabo, or the Sierras
103 Pintada and Las Cruces, east of La Paz (Fig. 1). A late Pleistocene – Holocene age range has
104 been obtained for the uppermost alluvial units correlated with El Chorro Formation near La Paz
105 (Maloney, 2009; Busch et al., 2011; Umhoefer et al., 2014) although no absolute chronology has
106 been developed for the older sediments, or for any of the sediments in the San José basin.

107 We studied in detail sediments of the above mentioned formation for the two most
108 extensive basins, La Paz and San José (Fig.1). Advantages of these locations include similarities
109 in parent material for regolith and sediments, in thickness of deposits, and in areal extent of
110 alluvial fans. Modern precipitation rates vary between 130 mm/year in La Paz to 340 mm/year in
111 San José del Cabo (Fig. 1), and relief in the catchments supplying these basins varies between
112 500 m in La Paz to 1500 m in the northern San José basin.

113

114 3. Methods

115 Mapping and identification of alluvial units was based on analysis of 1:20,000 aerial
116 photographs (INEGI, Mexico), and on Quickbird® and Landsat™ imagery over a base map
117 produced from a 10 m DEM (INEGI, Mexico), assisted by field characterization using excavated
118 pits, trenches and natural exposures. Alluvial stratigraphy was characterized along exposed
119 sections to identify buried soils or erosive surfaces that indicate depositional breaks or
120 stratigraphic unconformities. Detailed field descriptions of soil horizons developed on the most
121 stable surfaces were used to provide a relative chronosequence for the deposits and guidance for
122 cosmogenic depth profile and luminescence dating strategies. Sedimentary sections were

123 described in detail, relating the exposures to published facies descriptions (Miall, 1996, 2000)
124 and studying its variation along longitudinal or transversal location in the studied fans.

125 Multiple chronological methods were applied to the various studied sections to build a
126 robust chronological framework. Feldspar Infrared Stimulated Luminescence (IRSL) was used to
127 determine chronology of all units. Samples were taken from below the mixing some biological
128 or pedological processes, which was determined by observing soil textural and structural
129 properties in the upper zones of sampled sections, with field determinations being critical to
130 approve a site for luminescence or cosmogenic depth profile sampling. Single grain IRSL
131 methods on sand (180-220 micron size) were preferred because of expected incomplete
132 bleaching in this alluvial setting (Rhodes, 2011; Brown et al., 2014). Pilot samples were used to
133 establish optimal measurement conditions and fading properties (Huntley and Lamothe, 2001;
134 Brown et al., 2014). Dose recovery experiments were also performed to validate our approach
135 (Wintle and Murray, 2006). Sample preparation was carried out under dim filtered light
136 conditions at the UCLA and DRI Luminescence Laboratories. IRSL measurements were made
137 using TL-DA-20 Risoe automated readers; details on stimulation sources and emission filters can
138 be found in Table S-1 (See Supplementary Data File). A total of 51 samples were selected for
139 this study (Fig. 2). A direct comparison with cosmogenic age estimates was possible using
140 samples from the same pit profiles. A complete methodological description and discussion of the
141 feldspar luminescence approach is described in Brown et al. (2014). Radiocarbon dating was
142 performed on samples obtained from selected sites in younger units. Analyses were carried out
143 by Beta Radiocarbon, Florida. Radiocarbon dates were calibrated using Calib7.1 working with
144 INTCAL13 database (Reimer et al., 2013). Depth-profile measurements of cosmogenic nuclides
145 in vertical sections (e.g., Clapp et al., 2001; Frankel et al., 2007) were used to estimate
146 simultaneously cosmogenic nuclide inheritance as well as exposure age and erosion rate of
147 surfaces (e.g., Brocard et al., 2003; Hidy et al., 2010). ^{10}Be isotopes were analyzed in quartz sand
148 (355–710 micron) samples from well characterized alluvial fan surfaces (Fig. 2), with on-site
149 sieving to optimize sample amount according to expected AMS ratios based on preliminary
150 estimates of age (e.g., Gosse and Phillips, 2001). Initial preparation of samples for cosmogenic
151 analysis was performed at the Quartz Purification Facility at DRI. ^{10}Be was isolated from pure
152 quartz using chromatographic columns and chemical extraction at the Dalhousie Geochronology
153 Centre. Resulting BeO targets were analyzed at Lawrence Livermore National Laboratory

154 (LLNL). We use a constrained Monte Carlo approach to analyze TCN depth profile results,
155 coded in Matlab®. This code allows explicit input of geologic variables as surface erosion rate
156 and subsurface density and their probability distributions, reflecting uncertainties from field and
157 laboratory analyses (Hidy et al., 2010), in order to model reported surface ages.

158

159 4. Results

160 4.1. Soils data and geochronology

161 Time-related differences in composition, sedimentology, surface morphology and major soil
162 properties obtained from 21 described soil profiles for the major alluvial units identified was
163 compiled and integrated into a summary table (Table 1). Details about location of all soil pits,
164 sections and geochronology sampling sites are presented in Table S-2 (Supplementary Data
165 File). Geochronology results for luminescence dating are shown in Table 2, for radiocarbon
166 dating in Table 3, and for the two cosmogenic depth profile chronologies in Tables 4 and 5. The
167 temporal distribution of the six new IRSL ages and the C-14 and cosmogenic data is in
168 agreement with that of the chronology presented in Brown et al. (2014), and of previous work in
169 the La Paz and San Juan area (Maloney, 2009; Busch et al., 2011; Umhoefer et al., 2014).
170 Further details on interpretation of specific sites are presented below in the respective unit
171 description.

172

173 4.2. Characteristics of alluvial units

174 Six alluvial morphostratigraphic units spanning deposition from ~120 ka to the present
175 were identified in both studied basins. These units are described in detail below.

176

177 4.2.1. Unit Qt1

178 Alluvial unit Qt1 appears in the extreme northern and southern portions of La Paz basin.
179 In the north, unit Qt1 occurs as isolated patches remaining on slopes north and northeast of La
180 Paz, commonly within protected round-topped ridgeline remains in an example of ballena
181 topography (Driscoll et al., 1984) either overlying Oligocene fluvial conglomerates along the
182 coast (Fig. 3A) or entrenched, as in Coyote Valley (Fig. 2). Deposits assigned to Qt1 appear in

183 the southern portion of La Paz basin, outside of the mapped area (Fig. 2), composing most of the
184 moderately dissected and faulted fan morphology near La Matanza (Fig. 1), halfway between La
185 Paz and Todos Santos. In this area, the soil has been partially stripped, exposing a ~1 m thick
186 well cemented and indurated Bqm horizon, with evidence of silica precipitation in the matrix of
187 pebbly sand layers (Fig. 3B).

188 Polymictic rounded gravels are prevalent in the few natural exposures and road cuts that
189 expose unit Qt1 across Coyote Valley, in northern La Paz basin. The sediments in this part of the
190 basin are mostly derived from nearby Oligocene conglomerates bearing volcanic lithologies, as
191 opposed to the intrusive lithologies that dominate all rest of sediments in this study.
192 Sedimentology of this unit is dominated by gravels and sands with horizontal planar bedding and
193 imbrication indicating a northward flow in the Coyote Bay exposures (Fig. 3A), with similar
194 flow direction as the present-day Coyote Creek drainage. A soil section was excavated in a
195 preserved surface of the Qt1 alluvial deposit on top of a pronounced terrace that is ~15 m above
196 sea level along the western margin of Coyote Bay (pit REC-1; Fig. 2; Fig. 3C). This terrace
197 extends to the east of Coyote Bay, but in this area the upper alluvial level is missing in the
198 section and the soil is directly developed over littoral deposits (Fig. 3A). The alluvial deposit in
199 western Coyote Bay is ~5 m thick over a coral debris-covered marine abrasion platform, in turn
200 developed over more alluvial gravels. The soil here is deep (> 3m) and well-developed, and has
201 formed in sandy-gravel alluvium with a strongly-developed Bt horizon that has a well-defined
202 prismatic and angular blocky structure, a 5YR hue, and a clay loam texture. The soil also has a
203 strongly developed Bk horizon with stage III-IV carbonate that is weakly cemented in places
204 (Table 1; Fig. 3C). The source of the carbonate is probably from the in-situ dissolution of marine
205 calcareous materials (e.g. shells, corals) that locally comprise the base of the unit. The Qt1 soil
206 is the only soil described that has pedogenic carbonate. The soil of the Qt1 terrace is also the
207 best developed soil we have found in the study area that remains preserved at the surface (Table
208 1). In places (e.g., near Tecolote) however, the upper horizons of soil in this unit have been
209 completely stripped and only the harder Bk horizon remains.

210 Coral rubble and beach pebbles appear interbedded in the lower portion of the studied
211 Qt1 deposits at West Coyote Bay. Nearby, at Tecolote, the coral rubble has been dated by U/Th
212 to 146 ± 9 , 135 ± 6 ka (Szabo et al., 1990) and 123 ± 6 ka (Sirkin et al., 1989). Similar deposits on
213 the western La Paz Bay (outside of the area covered by Fig. 2) have been dated to 128-130 ka

214 (Forbis et al., 2004), all temporally related to a marine highstand during the interglacial Marine
215 Isotope Stage (MIS) 5e. We therefore interpret the age of the Qt1 deposits to be ~ 120-130 ka
216 (the age of marine highstand during interglacial stage 5e) because of the lack of soil formation in
217 the well-preserved coral rubble that is interstratified within the alluvium. This stratigraphic
218 relation indicates that limited time occurred between exposure of the deposits of the marine
219 incursion and subsequent burial by the alluvium. Deposition of unit Qt1 in northern La Paz
220 probably ended shortly after MIS 5e. We correlate the southern with the northern La Paz Qt1
221 deposits mainly based on soil development.

222

223 4.2.2. Unit Qt2

224 Alluvial unit Qt2 is an extensive deposit, especially along the southern La Paz basin and
225 the northern San José basin (Fig. 2). Unit Qt2 sediments appear in most places directly on top of
226 Pliocene sandstones in both basins, and is inferred to be stratigraphically on top of Qt1 deposits.
227 The contact with the Pliocene sediments can be observed at the foot of hillslopes along the
228 integrated drainage network that has developed on Qt2. In proximal fans, thickness of Qt2
229 sediment can reach up to 30-40 m. (Fig. 3D). The thick alluvial packages of Unit Qt2 produce
230 prominent fans, commonly inset by or overlain with younger alluvial units (Fig. 2, 3E).
231 Extensive erosion of Unit Qt2 has created ballena topography in places. Most Qt2 sediments are
232 derived from highly gneissified Cretaceous granites, granodiorites and tonalites. In the northern
233 edge of the San José basin some of the Qt2 sediments are derived from gneisses and quartz-
234 schists, and the sediments display a bouldery-blocky appearance (Fig. 4). Cobbles and pebbles
235 are the dominant grain sizes and are deposited as horizontal, lenticular or planar crossbedding
236 sets. Occasional pebble sand bars and medium sand lenses appear suggesting conditions of
237 reduced energy in the flow. Planar bedding is the most common sedimentary feature, along with
238 low-angle cross-bedding, with foresets and backsets (Fig. 4), and gravel bars. In some of the
239 coarser facies in this unit (e.g., in the northern San José basin), pool-and-chute features are
240 preserved in the sediments (Fig. 4).

241 Two sections were cleared and deepened on a quarry excavated at Ejido Alvaro Obregón,
242 La Paz Basin (Fig. 2). The soil formed in Unit Qt2 consists of a well-developed profile that has
243 formed in sandy-gravel alluvium, is nearly 3 m deep, and has a strongly-developed Bt horizon

244 with prismatic and angular blocky structure, a silty-clay loam texture, and a reddish hue 2.5YR
245 (Table 1; Fig. 5E). A cosmogenic depth profile from one of the described soils (EAO-3; location
246 in Fig. 2) yielded an age of 57.6_{-17}^{+19} ka (2-sigma) (Fig. 5). Similar IRSL ages were obtained by
247 sampling the same profile site at 2.7 m (57.2 ± 4.4 ka), and in a section 3 km south of the profile
248 site (48.0 ± 4.1 and 61.6 ± 5.6 ka), below a channel excavated into Qt2 filled with sediments
249 grading to Qt3 deposits (Fig. 3E). In San José, deposits mapped as Qt2 based on their soil
250 development and morphology yielded IRSL ages between 54.8 ± 5.5 and 65.6 ± 6.7 ka (Table 2).

251

252 4.2.3. Unit Qt3

253 Alluvial unit Qt3 is present across most of the study area either exposed at the surface or
254 overlain by younger alluvial units and exposed by stream or road cuts. As in the case of Qt2,
255 sediments for unit Qt3 are mostly derived of highly gneissified Cretaceous granites, from low
256 relief areas in La Paz basin, or from higher relief areas in San José. Locally, catchments with
257 gneiss and schist bedrock develop bouldery deposits as in northern San José. Unit Qt3 sediments
258 in places form a thick stack (~10-20 m) of sediment packages separated by weakly developed
259 oxidation zones (Fig. 6A). In some areas, the top of Qt3 is covered by thin (<5 m) layers of Qt4
260 sediments; the best example of this superposition is in San Lázaro (Figs. 2C, 6B, C), north of San
261 José del Cabo. In areas closer to the Holocene and modern-day active drainage network, Qt3 can
262 be covered by Qt5 deposits filling channels following closely the direction of drainages (Fig.
263 3E).

264 Coarse pebbles and cobbles in horizontal, lenticular or planar crossbedding sets dominate
265 the sedimentology of the Qt3 sections. Pebble-sand sets appear in 10-20 cm packages displaying
266 normal grading, with conformable or slightly erosive boundaries. The finer portion of these
267 packages is generally composed of medium sand. Planar bedding is the most common
268 sedimentary feature, along with low-angle cross-bedding, with foresets and backsets, and gravel
269 bars. The presence of transverse ribs (transverse gravel bars; cf. Allen, 1982), with boulders at
270 the top of 2 m packages suggest very energetic flow and development of standing waves (Fig. 4).
271 Lenticular and planar crossbedding sets in places develops characteristic antidune bedsets of
272 wavelengths up to 10-15 m. Event packages form sequences 1-2 m thick that can stack up to tens
273 of meters separated by well-defined erosional boundaries noted above. Maximum observed
274 thickness is about 20-30 m, especially in San José basin (San Lázaro, La Palma, Fig. 2, 6A).

275 Paleocurrent distribution from imbrication measurements indicates flow in a similar fashion to
276 the present-day fluvial conditions associated with floods generated by tropical storms. Trough
277 cross-bedding only appears towards the distal sections of the fans.

278 Soils formed in Unit Qt3 are deep (2.4-3.3 m) moderately developed soils that have a
279 moderately developed Bt horizon with weak prismatic to moderate subangular blocky structure
280 and 10YR to 8.75YR hues (Table 1). The soil profiles examined in the San José basin are
281 slightly better developed relative to soils in the La Paz basin due to a precipitation gradient that
282 increases to the south. A cosmogenic ^{10}Be profile age of 37.1_{-12}^{+13} ka (2-sigma) was obtained
283 in pit EAO-2 (Fig. 2), excavated at the southern portion of La Paz basin (Fig. 5). IRSL ages in
284 the same pit yield slightly younger dates when corrected for fading (31.0 ± 3.5 and 26.4 ± 3.4 ka).
285 All IRSL ages in San José basin match the depth-profile cosmogenic age range in the above
286 mentioned EAO-2 pit (30.6 ± 2.8 to 37.0 ± 2.9 ka).

287

288 4.2.4. Unit Qt4

289 Alluvial unit Qt4 is exposed as an extensive unit with outcrops comprised of depositional
290 layers 5-10 m thick that overlie sediments of unit Qt3 in San José (e.g., Arroyo San Lázaro, Fig.
291 6B-C). In the Cajoncito alluvial fan in La Paz, 10-15 m of exposed section is partially covered by
292 1-3 m of Qt5 sediments (Fig. 6E). In the rest of northern La Paz basin, most of the unit appears
293 to be blanketed by a layer of Qt5 deposits.

294 Most sections are dominated by coarse sand and fine pebble sheets with varying
295 proportions of coarse pebbles and cobbles in horizontal, lenticular or planar crossbedding sets
296 which in places form characteristic antidune bedsets of wavelengths up to 10 m. Planar bedding
297 is the most common sedimentary feature (Fig. 6B,E), along with low-angle cross-bedding, with
298 foresets and backsets, and gravel bars. Pebble-sand sets appear in 10-20 cm packages displaying
299 normal grading, with conformable or slightly erosive boundaries. The finer portion of these
300 packages is generally composed of medium (rarely fine) sand. The packages form sequences 1-2
301 m thick that stack up to tens of meters. It is rare to observe more than ~10-15 m of cumulative
302 deposition in section, and clear stratigraphic boundaries appear beyond this thickness with Qt3
303 below (especially in San José) and Qt5 on top (especially in La Paz). Palaeocurrent distribution
304 from imbrication measurements indicates channel networks that drained in similar fashion to the
305 present-day conditions.

306 The Qt4 alluvium has a stable soil on the surface (e.g., in San José) or is overlain by the
307 younger unit Qt5 (e.g., Cajoncito, La Paz). Unit Qt4 is identified in the field due to a deep (>2.5
308 m) moderately developed soil profile that is easily distinguishable from soils developed on the
309 Qt5 or Qt3 deposits. Four soil profiles with similar morphology were described (e.g., Table S2 in
310 the Supplementary Information Dataset, pits SJ1, SJ2, ST1, ST2). The typical unit Qt4 soil
311 (Table 1) has formed in sandy-gravel alluvium (Fig. 6C-D) and is a deep, moderately developed
312 soil with either a weakly developed Bt horizon or a distinct Bw horizon. The soil contains
313 abundant faunal burrows and root casts up to 150 cm deep. IRSL ages on Unit Qt4 range from 18
314 to 6 ka (Table 2), although most of the deposits are in the range 15-11 ka. The upper 2 m of
315 several dated pit and section profiles (e.g., SJ2; Fig. 6D) have younger (7-3 ka) ages than the
316 bulk of the deposits sampled along natural sections. Ages less than ~ 7 ka from these profiles are
317 most likely due to unrecognized bioturbation and the downward mixing of soil from the surface
318 rather than representing a separate overlying Qt5 deposit. The overall depth and structure of the
319 Bt horizon in the upper 2.5 m at all four sites is very similar, there are no clear signs of fluvial
320 truncation and/or deposition of younger sediment within any of the Qt4 sections examined, and
321 the soils on unit Qt4 within the uppermost 1.5-2 m are deeper and distinctly better developed
322 than the Qt5 soils (Table 1), as discussed below. By comparison, the degree of soil development
323 indicates that a distinct Qt5 layer overlies the Qt4 in the La Paz basin, indicating that the Qt4
324 surface was subsequently covered by Qt5 (Fig. 6E).

325

326 4.2.5. Unit Qt5

327 Unit Qt5 is associated with the drainage network linked to present-day arroyo
328 development, in two characteristic settings. First, it appears infilling 0.5-2 km wide channels
329 with terraces that are about 2-3 m above modern channel level (Fig. 7A-B). Second, unit Qt5 in
330 La Paz basin overtops channel banks and blankets Qt4 sediments with a variable thickness of
331 sediments (Fig. 7E), aggrading to the same level than unit Qt6 in distal alluvial fan positions
332 south of the city of La Paz. Units Qt5 and Qt6 are difficult to separate when viewing imagery
333 and criteria for distinguishing them are based on their position in the present day landscape, type
334 of vegetation cover, and relative differences in soil development. Without geochronological
335 control of every section, misidentification is possible.

336 Coarse sand and fine pebble sheets dominate the sediments, in horizontal, lenticular or
337 planar crossbedding sets. In La Paz, cobbles and pebbles occur rarely and are restricted to the
338 base of individual packets, while in San José cobbles and boulders are more common, especially
339 towards the north, where overall deposits are coarser. Pebble-sand sets appear in 10-20 cm
340 packages displaying normal grading, with conformable or slightly erosive boundaries. The finer
341 portion of these packages is generally composed of medium (rarely fine) sand. The packages
342 form sequences 1-2 m thick that appear stacked, separated by well-defined erosional boundaries
343 from Qt4 or older units (e.g., Fig. 3D), and with cumulative thickness of maximum 5-6 m (e.g.,
344 east of La Paz, section CAN-1). Planar bedding is the most common sedimentary feature,
345 although massive sediment packages and planar cross-bedding have been observed (Fig. 7C-D).

346 Soil stratigraphy indicates that unit Qt5 can be subdivided into 2 distinct alluvial units
347 (Table 1) and that each of these soils is readily differentiated from soils on either the Qt4 or Qt6
348 surfaces. Units Qt5o and Qt5y have however not been differentiated in our mapping (Fig. 2) due
349 to a lack of correlation between surface morphology, position in the landscape and the above
350 mentioned features. It is also possible that unit Qt5o is expressed as a separate deposit only in La
351 Paz. Soils on the Qt5o (older) surface are nearly 1.5 m thick and have a moderately developed
352 Bw horizon with weak to moderate subangular blocky structure, loamy sand texture, and 10 YR
353 hues. By comparison, the soils formed on unit Qt5y (younger) are less than 0.6 m, have a weakly
354 developed Bw horizon, with weak subangular blocky structure in a few horizons, and a sandy
355 texture. The Qt5 unit chronology ranges between ~2.5-6 ka, which we correlate to the soil-
356 defined unit Qt5o (e.g., Mesquitito, Bonfil bank, Table 2, Fig. 7D), to 0.3-0.4 ka, which is
357 correlated to unit Qt5y (channel inset terraces in La Paz and San José). The latter chronology
358 overlaps with unit Qt6 (Fig. 7B). In the Mesquitito ¹⁴C/IRSL profile (Fig. 2, 7D), Qt4 and Qt5
359 units are separated by a buried soil with a weak Bw, corresponding also to the change observed
360 in the absolute chronology.

361

362 4.2.6. Unit Qt6

363 Unit Qt6 appears in natural sections and man-made excavations along the drainage
364 network associated with recent arroyo development. Its largest extension is reached in the distal
365 portions of alluvial fan complexes in La Paz basin. In San José basin this unit is restricted to

366 channel infilling (Fig. 7A-B). Two settings can be distinguished. One is the active channels,
367 which are occupied by tropical cyclone or other summer precipitation-derived runoff at least
368 once or twice per year, mostly near the mountain fronts (Fig. 7B). The other is vegetated bars
369 and 1-2 m high terraces along the channels that are completely flooded and reshaped once every
370 three to five years when a major tropical cyclone affects the region (e.g., Hurricane Juliette in
371 2001; Farfán, 2004). Occasionally, flooding from large tropical storms has spilled sediment over
372 channelized banks, as it happened during hurricane Liza in 1976 in La Paz basin (Fig. 8). The
373 streamflow during this storm bifurcated and occupied the northernmost channel of Arroyo
374 Cajoncito when entering the urban area of La Paz, funneled by two nearby hills, destroying a
375 retention dam. Along the channel banks, in the apical fan area, more than three meters of
376 sediment, including large cobbles and boulders, along with assorted anthropogenic material
377 (glass shards, concrete pieces, rubber tire pieces, tin cans) were deposited (Fig. 8A,D). At least a
378 meter of sand and coarser sediment was deposited along specific alluvial channels in the urban
379 area of La Paz, which together with the flooding caused the death of around 600 people
380 (Villanueva, 2001). Active, channelized runoff over the surface of alluvial units Qt4 and Qt5 has
381 been documented by aerial photographs taken shortly after the event east of La Paz (Martínez
382 Gutiérrez and Mayer, 2004), indicating that infiltration capacity was exceeded during this storm
383 even for these sandy younger units.

384 Characteristic horizontal bedding is observed in sediments of Qt6 (Fig. 8B, D). Upstream
385 and downstream dipping low-angle planar cross-bedding in antidune bedforms with 2-4 m
386 wavelength is also observed particularly near the base of the Liza deposit in Cajoncito, along
387 with massive gravels (Fig. 8C). Sediments mapped as Qt6 have minimal soil development which
388 primarily consists of a weak accumulation of organic matter and soil mixing from faunal and
389 flora bioturbation. Luminescence chronology indicates 1.0-0.1 ka for Qt6 sediments along the
390 channel and the lowest terrace in both basins (Table 2), even for sediments deposited during
391 hurricane Liza (Fig. 8C).

392

393 5. Discussion

394 5.1. The alluvial chronosequence

395 Alluvial deposition in the study area took place along fans radiating out of the mountain
396 fronts defined by La Paz and San José faults (Fig. 1). The alluvial deposits exhibit sequences

397 that are regional in scope and comparable to alluvial deposits in other areas of southwestern
398 North America, like the northern Sonoran desert (cf. Bull, 1991; Spelz et al., 2008; Armstrong et
399 al., 2010), where Pleistocene alluvial fans have been interpreted as developing in response to
400 climate variation (Bull, 1991). Sedimentary units in the study area correlate across the two
401 studied basins (Fig. 2), indicating a common mechanism of generation, independent from both
402 the tectonic evolution of specific uplifted ranges (Sierra La Laguna and Sierra La Pintada) and
403 present day differences in total precipitation. Similarity in alluvial aggradation timing for the two
404 different basins also suggests a common response to a driver other than base level change (sea
405 level in this case). If sea level were an important driver (more than local expression of climate),
406 active deposition would appear in La Paz basin during the low sea level period associated with
407 the global last glacial maximum (LGM). We note that the shelf in this area has a much lower
408 slope than the overall alluvial plain (cf. Del Monte-Luna et al., 2005) and therefore any fall in
409 sea level would have caused aggradation (cf. Summerfield, 1985; Leckie, 1994), not incision.
410 The response in San José during the LGM on the other side, should have been of a deep incision
411 of previous surfaces (Qt3, Qt2), given that the shelf has a short, steep slope. Deep channels are
412 excavated, but they not only incise Qt2 and Qt3 units but also thick Qt4 deposits blanketing
413 previous units, and therefore these channels postdate the LGM. Incision therefore is at least post-
414 9-11 ka in both basins (Qt4). In La Paz, incision probably only happened after Qt5o (5-6 ka).

415 Regional stratigraphic units can therefore be interpreted as pronounced aggradational
416 events (Fig. 2) related to time-transgressive changes in climate. Cycles of increased
417 sedimentation and subsequent channel incision produced distinct, commonly extensive
418 geomorphic surfaces. In most places these surfaces are preserved today, although in places
419 sediments of older units are buried by thin mantles of younger units, as in Qt5 over Qt4 in La Paz
420 (Fig. 2, 6E, 7D), or in Qt4 over Qt3 in San José (Fig. 2C, 6B). Evidence for periods of deep
421 incision is apparent between Qt4 and Qt5 (up to 30-40 m in San José, 10-20 m in La Paz), and
422 Qt5 and Qt6 in La Paz (~10 m). Between Qt2 and Qt3 in San José basin, channel incision and
423 sediment burial is recorded without the impressive (>20 m) incision characteristic of the
424 channels where younger (Qt4, Qt5) units are incised. Paleochannels interpreted as developed
425 during Qt3 appear nevertheless in similar position and orientation as present-day channels (Fig.
426 2). Synchronic incision in both basins suggests that tectonics and sea level change (as base level
427 change) are not primary drivers of this incision. We propose instead, as a working hypothesis,

428 that incision of fan surfaces in this area is caused primarily by a reduction in the amount of
429 sediment produced and supplied by hillslopes between major aggradation periods, linked not
430 only to a potential reduction in runoff but also to a climatically induced reduction in sediment
431 production under relatively colder and drier conditions (cf. Hidy et al., 2014).

432

433 5.2. Evidence for intense rainfall events

434 A difference between the alluvial sequence analyzed in this study and that in the northern
435 Sonoran desert however is the lack of bar and swale topography commonly observed in the
436 Sonoran and Mojave deserts (cf. Bull et al., 1991; Miller et al., 2010). Bar and swale topography
437 is not prevalent on the surface morphology for most of the alluvial fan surfaces, except in
438 reduced areas of the youngest (Qt5-Qt6) deposits. Bioturbation in both the higher alluvial
439 surfaces in La Paz and across the entire San José basin could have caused reduction of the small-
440 scale relief. We observe however that the sedimentology of the units does not support any
441 braided stream activity in the fans, as noted in the Lower Colorado (Bull, 1991). Trough
442 crossbedding, for example, was only observed in one place in unit Qt3, restricted to the lower
443 portion of the fan units near Caduaño (Fig. 2).

444 Present-day climatology indicates that extreme rainfall events in the region (i.e., P95
445 events, those whose total precipitation is above the 95% of all events) leave a geomorphic legacy
446 of erosion, flooding and landsliding (Martinez-Gutierrez and Mayer, 2004; Raga et al., 2013;
447 Antinao and McDonald, 2011; Antinao and Farfán, 2013), and they are all derived from tropical
448 cyclones (Englehardt and Douglas, 2001; cf. Diaz et al., 2008). Similarity in sedimentology
449 between historical (Qt6) and older units (Table 1B) is arguably proof that deposition of older
450 units was achieved by storms of at least similar intensity and duration, and that the regionally
451 high-intensity rainfall associated with tropical cyclones provides the source for such energetic
452 and prevalent flow, as compared e.g., with rainfall from convective sources during summer time
453 and associated with the NAM only.

454 A quantitative estimate of instantaneous paleodischarge was performed using techniques
455 developed by Kennedy (1961, 1969) and Foley (1977), using measured wavelengths in preserved
456 antidune bedforms of upper-flow regime lithosomes, and estimates of channel widths based on
457 directly measured or similar medial or apical channel dimensions in the basin (Table S-3).
458 Instantaneous discharge estimates average $\sim 10,000 \text{ m}^3\text{s}^{-1}$ e.g., for sections in San José Qt3 unit

459 (Fig. 4; Table S-3), approximately one order of magnitude higher than instantaneous discharges
460 from recent storm hydrographs in the same catchment (e.g., those measured during hurricane
461 Paul in 1981 by Bonillas, 1984). Extreme values up to $23,000 \text{ m}^3\text{s}^{-1}$ were calculated for some
462 individual sections in the same catchment (Table S-3). For the Cajoncito sections measured in
463 deposits left by tropical storm Liza in 1976, our estimate is $\sim 3,000 \text{ m}^3\text{s}^{-1}$ (Table S-3) a figure
464 consistent with the hydrograph measurements by Bonillas (1984) on hurricane Paul in 1981.

465 Facies in the historical deposits generated by tropical cyclones –for example those
466 deposited during tropical storm Liza in La Paz (Fig. 8, Table S-3) — are equivalent with those
467 observed in Pleistocene – Holocene sediments in units Qt2 through Qt5, although a progressive
468 reduction in magnitude of floods is evident from the diminished preservation of antidunes and
469 transverse ribs in the younger Qt5 and Qt6 deposits (Table 1B). We deduce that deposition of all
470 units occurred rapidly during intense or long duration tropical cyclones approaching or making
471 landfall in the southern peninsula. Our record suggests therefore that variations in climate
472 conditions during specific, discrete periods in the last 70 ky allowed tropical storms to become
473 both more intense and more frequent over the southern peninsula. These conditions waned
474 during specific portions of the time period analyzed, and specifically, during the Holocene,
475 driving finally the frequency and intensity of tropical cyclones to those similar to observed in the
476 present day.

477

478 5.3. Evolution of depositional events in the record

479 The overall thickness of the sediment units diminishes from the Pleistocene (Qt2)
480 throughout the Holocene (Qt5-6) fans (Figure 2; Table 1), similar to the evolution of the lower
481 Colorado alluvial fans (Bull, 1991). Based on the observed bedforms (Table 1B) and compared
482 to sediments of alluvial fans formed under conditions of rapid sedimentation and high discharges
483 (cf. Duller et al., 2015), conditions prevailing during Qt2 through Qt4 were of larger sediment
484 supply than Holocene to present-day conditions, along with active fan deposition. Thicknesses of
485 tens of meters of sediment were deposited at locations in the middle and distal portions of the
486 fans (Fig. 3D, 6A), contrasting with the reduced (<10 m in general) thickness on the Holocene
487 units (Fig. 7). The lack of transverse gravel bars (transverse ribs) in units Qt5 and Qt6 (Table
488 1B) also suggests a progressive reduction in maximum energy flow events since the Late
489 Pleistocene. Horizontal plane bedding and characteristic antidune bedforms are retained however

490 in the sedimentology throughout the Holocene units, albeit with reduced wavelengths (compare
491 Fig. 4 with Fig. 8). We conclude that the Holocene has witnessed potentially less and less intense
492 arrival of cyclones than the late Pleistocene, although it did not lack completely arrivals,
493 demonstrated by historical tropical storms Liza in 1976 and Juliette in 2001, among others (cf.
494 Ragas et al., 2013; Villanueva, 2001; Antinao and Farfan, 2013).

495

496 5.4. Self-channelization

497 Self-channelization is evident in older units away from the outlet of major bedrock
498 catchments. We hypothesize that as these surfaces get older, surface erosion results in the
499 formation of a ridge-and-channel topography that eventually evolves into ballena topography.
500 Temporal changes in surface topography are most likely related to soil profile development (e.g.,
501 silt and clay content increase) that tends to decrease surface infiltration and increase surface
502 runoff, enhancing concentration of surface water into channels between interfluves. This process
503 occurs however at a lesser scale in surfaces with low relief, like the younger Qt4 or Qt5. These
504 surfaces are extensive enough in the landscape (Fig. 2) that occurrence of intense rainfall events
505 might lead to surface flow, considering their high infiltration capacity. An example of surface
506 flow in areas without obvious channels has been observed in historical storms like hurricane Liza
507 in 1976. During this storm, small channels formed on the surface of the Qt4-Qt5 fan, away (1
508 km) from the main channel, and deposited sediment at distal positions in the fan without any
509 upland bedrock catchment to source the water or the sediment. Reworked sediment might be
510 eroded, transported and deposited in 0.5-1 m hollows, and landscape scars are rapidly healed
511 with vegetation activity afterwards (cf. Antinao and Farfán, 2013, for similar observations on
512 landslides). This effect might also partially explain some of the younger ages on the higher
513 portion of Qt4 soil pit age profiles in San José (Fig. 6D, pit SJ2; also pit ST2, Table 2, and Table
514 S-2). In any case, the amount of sediment redeposited on distal sites during historic storms is
515 small compared with the amount deposited in the main channels feeding sediment from upland
516 catchments, and we consider the effects of self-channelization to be more relevant for the
517 progressive toe erosion of fans, than for fan surface development (i.e., no subsidiary fans
518 developing from fan medial sites).

519

520 5.5. Cosmogenic ^{10}Be depth profile results

521 Cosmogenic ^{10}Be depth profiles indicate the age of the stabilization of the surface being
522 analysed, giving also useful information regarding the isotope content inherited during previous
523 transport and hillslope storage. Observed change in ^{10}Be concentration with depth was similar for
524 both profiles, and deviations from an ideal exponential profile in EAO-2 can be explained by
525 mixing in the upper layers of the profile by pedogenic processes not observed in the field. These
526 mixing processes were nevertheless confirmed by other pit age sequences (cf. shallow Qt4 IRSL
527 profiles in San José), and were restricted to the upper 50 cm of the pit. Sediment density analyses
528 in the lab and the field yield density curves (Fig. 4B, F) that were used as input for the model, as
529 cumulative densities. The density curve was consistent with expected pedogenic evolution from
530 the parental material. For profile EAO-2, model runs including and excluding the upper two
531 samples were performed in order to understand the effect of the mixing in the final model age.
532 No improvement in uncertainty was found when running only the lower samples, and therefore it
533 was decided to include all samples in the modeling effort. Consistency with one of the IRSL ages
534 at 1-sigma, from a sample below the mixing zone, suggests that indeed the age of sedimentation
535 and surface stabilization are very close.

536 The anomalously high ^{10}Be content of the second shallowest sample for EAO-3 is linked
537 to an anomalously high density value that we associate with disruption of the horizon by subtle
538 bioturbation at a deeper level in this older unit. Running the profile model without this sample
539 data point does not improve obtained uncertainties. The remarkable agreement between the
540 relatively deep IRSL sample and the profile age (Fig. 4) indicates stabilization occurring
541 immediately after deposition of the event.

542 The soil profiles indicated minimal surface lowering based on the presence of a complete
543 horization and pedogenic structures. The models showed in Figure 4 used as initial constraints,
544 besides the indicated density profiles, maximum lowering amounts of 10 cm for each profile.
545 Models returned however relatively flat distributions for erosion rates, with median values
546 around 0 cm/ky. Model inheritance values are in the same order of magnitude for both profiles,
547 with reduced uncertainties arising from the modeling of profiles with relatively deep (>2 m)
548 samples.

549

550 5.6. Chronology of events and evidence for discrete depositional periods.

551 As discussed above, rapid deposition is suggested by the sequence of ages in specific
552 sampled sections of Qt3 and Qt4, with cycles of rapid deposition recognized as distinct packages
553 of alluvium. Inside each package, ages agree at 1-sigma (e.g., Fig. 6C, E; Fig. 7C). Additionally,
554 although age estimates are in correct stratigraphic order for most of the dated samples, ages
555 nevertheless overlap at 1-sigma for two consecutive sediment packages (SL-III section; Fig. 4).
556 The chronology presented here in addition to that presented in Brown et al. (2014) allows us to
557 be confident about the ranges of deposition for the alluvial sediments in the study area. Our
558 interpretation is further supported by consistency of the chronology with that of Maloney (2009)
559 in the Carrizal fault system, western La Paz basin (Fig. 1), using Optically Stimulated
560 Luminescence (OSL) in quartz. Ages for their units Qya3 and Qya2 are consistent with our units
561 Qt4 and Qt5o, at ranges of ~13-7 ka and 6-1.3 ka. Soil data (this study) for the sites described in
562 Maloney (2009) are consistent with development expected given the time range determined for
563 surface stabilization of these units. Similarity of cosmogenic depth profile surface stabilization
564 ages to luminescence burial ages both at a regional scale (Fig. 9) and at the pit scale (Fig. 5)
565 indicate that sedimentation quickly stopped and was followed by a hiatus in deposition that
566 allowed soils to form. Development of soils that are clearly distinguishable between mapped
567 units (Table 1) at a regional scale and the well-defined chronology for Late Pleistocene units
568 (Fig. 9) is indicative of discrete periods when deposition occurred.

569 These discrete periods that we interpret as dominated by deposition are not separated by
570 sharp temporal boundaries from non-depositional periods. In a few cases ages in one unit overlap
571 with ages on the older or younger unit (Fig. 9), because alluvial units were mapped according to
572 a set of field criteria; besides the internal variability in age distribution in one unit, individual site
573 hydrological and compositional factors might have played a role in masking relative age
574 classification. We interpret periods when limited deposition is observed (e.g., around 20-30 and
575 40-50 ka) as having evolved like the Holocene, with reduced aggradation (in volume) that
576 nevertheless is still observed when the age of individual sediment packages is considered. For
577 sediments deposited during these periods, pedogenic and surface evolution from deposition to
578 the present-day developed very similarly to younger or older larger sediment packages, and
579 therefore we could not assign these sediments into distinct units, but instead decided to include
580 them into the larger packages.

581 Well-defined erosional boundaries separate each unit, from Qt2 to Qt6. These boundaries
582 include current exposed surfaces for all units (e.g., Fig. 2C). No distinct buried soils have been
583 identified within these sediment packages that would indicate a significant break in aggradation
584 inside identified units Qt2 to Qt6, which instead show tens of single depositional packages about
585 1-3 m in thickness separated by depositional or light cross-cutting relations. These individual
586 packages might be separated by a variable time gap that can range between decades to a few
587 millennia at most (Fig. 4). In the latter case, oxidised sandy layers can be identified as
588 stratigraphic markers (Fig. 6A). In the former case, and throughout all units, a change in
589 sedimentation conditions is the only indication of a separation between events, for example
590 grain-size changes or cross-cutting relations (Fig. 4, 8). The perceived intra-unit periodicity of
591 sedimentation mentioned above is based mostly in the lack of soil development and it is similar
592 with e.g., the periodicity interpreted for tropical cyclone-induced landsliding events, documented
593 for San José basin in Antinao and Farfán (2013).

594

595 6. A dynamic link to explain alluvial aggradation: implications for paleoclimate

596 6.1. Tropical Pacific forcing of alluvial cycles

597 The most important feature of the fan chronology (Fig. 9) is the cyclicity of deposition of
598 the thicker units (Qt2, 3, 4) that is correlative with the variation in summer insolation in an area
599 of the tropical Pacific where eastern Pacific tropical cyclones are generated (Fig. 9E). This
600 insolation variability is in turn, mostly controlled by precessional cycles (Berger, 1991). As far
601 as we know this is the first record that documents a precession-driven alluvial chronology for
602 southwestern North America. We propose that at these specific periods generation of more and
603 more intense tropical cyclones in the eastern Pacific basin was accomplished by a larger amount
604 of solar radiation received by the area of genesis of eastern Pacific tropical cyclones (i.e.,
605 between 10-20 N, Fig. 9E), accompanied by a weakening of the North Pacific High, hence
606 reducing the intensity of the California Current (cf. Roberts, 2004; Lyle et al., 2010) and
607 allowing the penetration of tropical waters, which has been documented at least for Qt4 times
608 (17-11 ka) for the region offshore Baja California (Rodriguez-Sanz et al., 2013). The proposed
609 mechanism has two competing features, as a northward movement of the Intertropical
610 Convergence Zone (ITCZ) drives a larger pool of moisture closer to southwestern North
611 America, but also a strengthening of the North Pacific High (NPH) that blocks advection of

612 tropical moisture into the continent. Effects of this proposed mechanism should be more
613 important mostly in the rising limb of the precessionally-controlled insolation curve, as we
614 observe in the southern Baja California record (Fig. 9F). Once the insolation maximum is
615 reached, the NPH is at its maximum strength and conditions for transport of tropical moisture are
616 reduced, not only for summer storms but also for winter extratropical cyclones.

617 The precessional cyclicity of the fan aggradation and associated correlation with high
618 summer insolation is in contrast with previous studies of alluvial fan deposition in the region,
619 interpreted primarily occurring in response to glacial-interglacial cycles. In these southwestern
620 North America studies, fan aggradation is interpreted to occur in response to either a southward
621 shift of westerlies winter storm band in response to disturbances caused to hemispheric
622 circulation patterns by the development of the high latitude ice sheets (cf. Spelz et al., 2008;
623 Armstrong et al., 2010; Owen et al., 2014), or as a result of enhanced activity of monsoonal
624 thunderstorms under an overall climate shift from wetter to dryer conditions during deglaciation
625 (e.g., Bull, 1991; Miller et al., 2010).

626 The three major aggradation units in the alluvial record described in this study (Qt2 to
627 Qt4) indeed correlate with periods of alluvial fan formation in both the Peninsular Ranges and
628 the Transverse Ranges in southern California and the northern Baja California peninsula (Fig.
629 9C; cf. Armstrong et al., 2010; Spelz et al., 2008; van der Woerd et al., 2013; McGill et al., 2013;
630 Blisniuk et al., 2012; Owen et al., 2014). A recent compilation of records by Owen et al. (2014)
631 also contains aggradation peaks at ~35 ka and ~65 ka. These mostly southern California records
632 are consistent with deposition during Qt2, Qt3 and Qt4, but also suggest that there is a LGM
633 component that is not observed in Baja California, which is reasonable, because we interpret that
634 sedimentation was triggered in Baja California by low latitude forcing that induced enhanced
635 tropical storm precipitation. Periods of aggradation in Baja California also correlate with periods
636 of increased runoff in a record from a high elevation southern California lake at ~36 ka and ~53
637 ka (Kirby et al., 2006; Fig. 9B), and similar records in lake systems across southwestern North
638 America (e.g., Laguna San Felipe, 13-9 ka, Lozano-Garcia et al., 2002, Roy et al., 2012; Lago
639 Santiaguillo, Durango, at 12.3-9.3 ka, Roy et al., 2014; Babicora, at 29-38 ka and 57-65 ka,
640 Metcalfe et al., 2002; Fig. 9B). Similar to the alluvial record mentioned above, we note that the
641 current interpretation of these lacustrine records is described as increased precipitation from
642 disparate sources, e.g., due to an enhancement of the North American Monsoon (e.g., Metcalfe et

643 al., 2002), or to south displacement of the westerlies (e.g., Roy et al., 2014) at different periods.
644 Lyle et al. (2010, 2012) have suggested that an increase in direct transport of tropical Pacific
645 moisture has been involved in hydrological changes for some of these lakes. The Baja California
646 alluvial record is consistent with this idea, in that alluvial fan data neither records westerlies or
647 monsoonal influences but instead direct tropical Pacific influence during the summer.
648 Consequently, our results provide an end-member perspective on a relatively unknown variable
649 in southwestern North America hydroclimate variability: eastern Pacific tropical cyclones. The
650 above discussed evidence for contemporaneous increase in effective moisture and runoff across
651 this subtropical region where several hydroclimates dominate is consistent with our record. This
652 temporal correlation suggests that a similar tropical forcing may play a role in the evolution of
653 these northern records and that in future analyses the incorporation into the discussion of the
654 tropical cyclone end-member is warranted in order to provide a more reliable assessment of the
655 hydroclimates of the region during the late Pleistocene.

656 We compared also our alluvial record to two records of terrigenous supply to the offshore
657 areas of southern California (ODP site 893; Fig. 1; Robert, 2004) and from the eastern Pacific,
658 off southwestern Baja California (core MD02-2508; Fig. 1; Blanchet et al., 2007). In the
659 southern California core, clay mineral assemblages indicating terrigenous supply were described
660 as modulated by summer insolation, with peaks at ~35 ka and ~60 ka (Robert, 2004; Fig. 9A).
661 The record of Robert (2004) also displays several maxima around the LGM and the late
662 Pleistocene – Holocene transition. In core MD02-2508, minima in the hard isothermal remnant
663 magnetization record (HIRM; Fig. 9D) can be used as a proxy for wet periods with increased
664 terrigenous supply, as opposed to high peaks in the record when wind-blown magnetic minerals
665 were brought into the core region under relative arid conditions and an enhanced anticyclone
666 regime. Wet periods appear around 10 ka and ~30-35 ka (Fig. 9D), coincident with our alluvial
667 record for Qt3 and Qt4. Beyond ~38 ka the HIRM record is only pinned by the Blake magnetic
668 excursion at ~120 ka (Blanchet et al., 2007), which complicates any correlation with the already
669 wide range of ages for Qt2 deposition. The striking relationship that must be highlighted is the
670 apparent control of the alluvial record by insolation variation in the area and season most prone
671 to genesis of tropical cyclones (Fig. 9E, F. This result emphasizes the potential for our record to
672 be used as a strong benchmark for discrimination of tropical influence on any other alluvial
673 record in southwestern North America.

674

675 6.2. Modulation by ENSO

676 The alluvial record described in this study shows a period of enhanced sedimentation
677 around 16-9 ka (Qt4 deposition, Fig. 9F). During this period, midden records for north and
678 central Baja California show displacement of chaparral associations to their southernmost
679 recorded position suggesting an increase of winter precipitation and a more equable, less
680 seasonal climate (Van Devender, 1997; Rhode, 2002), consistent with increased water levels in
681 present-day dry peninsular Lakes Chapala and Laguna San Felipe (Davis, 2003; Lozano-Garcia
682 et al., 2002). Coexistence of increased winter precipitation along Baja California during the late
683 Pleistocene-Holocene transition with more frequent arrival of large tropical storms is consistent
684 with more frequent El Niño-like conditions during at least the early portion of this period (e.g.,
685 Koutavas et al., 2002, Masters, 2006; Grelaud et al., 2009), because it might have shifted winter
686 storm tracks south as it does in the present day (e.g., Cayan et al., 1999). Although observations
687 in marine cores in the Gulf of California, and along the eastern Pacific including offshore Baja
688 California all support El Niño-like conditions during the late Pleistocene-Holocene transition
689 (e.g., Koutavas and Joanides, 2012; Staines-Urias et al., 2015), the lack of proxies documenting
690 unequivocally ENSO variability beyond that period precludes a more definite test of an
691 hypothetical connection between ENSO and advection of tropical moisture into southwestern
692 North America for the late Pleistocene. A precession-driven, coupled model describing sea
693 surface temperature anomalies in the equatorial Pacific, extending back into MIS 5 is only
694 partially consistent with the marine records described above for the late Pleistocene-Holocene
695 (Clement et al., 1999; Fig. 9G), and with the alluvial record described here, that appears to be
696 dominant only during the waning limbs of the NINO3 anomaly curve after maxima periods, even
697 extending to periods of minima (Qt3).

698 Present-day observations of the effects of ENSO on synoptic patterns in southwestern
699 North America however support a causative linkage between El Niño-like conditions and a
700 larger role of tropical storms in hydroclimatology of the region. The warm phase of the El Niño –
701 Southern Oscillation negatively affects North American Monsoon activity (e.g., Castro et al.,
702 2001; Gochis et al., 2007; Gochis and Berberry, 2011) At the same time, El Niño-like conditions
703 could have increased tropical cyclone activity in terms of intense (Category 4-5) hurricane
704 occurrence, similar to what has been documented during the last 50 years in the Eastern Pacific

705 Basin (e.g., Gray and Sheaffer, 1991; Elsner and Kara, 1999; Chu, 2004; Romero-Vadillo et al.,
706 2007; Raga et al., 2013). Although a few studies have found no influence from El Niño on the
707 total amount of cyclones (Cayan and Webb, 1992; Raga et al., 2013), there is a growing body of
708 literature that has actually found evidence for a positive effect of ENSO-warm phase on
709 occurrence of tropical storms (Rodgers et al., 2000; Jauregui, 2003; Jien et al., 2015).

710 As mentioned above, a northern, possibly wider, ITCZ at times of increased summer
711 insolation in the Northern Hemisphere (Haug et al., 2001; Koutavas and Lynch-Stieglitz, 2005;
712 Broccoli et al., 2006), would provide a larger amount of moisture to tropical cyclones, which
713 were also more likely to recurve northward and eastward given both the weakening of the North
714 Pacific High and the increase in cut-off lows both expected for El Niño or warm ENSO
715 conditions in the Eastern Pacific (Cayan and Webb, 1992).

716 It is important to note that all the above mentioned causal mechanisms are interconnected
717 and none should be flagged as a standalone cause for the proposed increase in advection of
718 tropical moisture into the coast of southwestern America. Warm ENSO conditions, although
719 important for generation and advection of tropical storms, are not sufficient to develop a pattern
720 of alluvial deposition by itself. The clustering of dates, which mostly appear between a NINO3
721 model maxima and an insolation maxima (Fig. 9) is interpreted as reflecting a sequence of
722 effects occurring during several thousands of years. First, an El Niño-like state in the tropical
723 Pacific benefits formation and arrival of strong storms directly, as stated above; second, as that
724 effect wanes, the insolation effect takes over and maintains the cycle of tropical moisture
725 advection active. Note that a reduction of activity around the LGM also can be attributed to the
726 still lingering effects of hemispheric cooling at a time when the continental icecaps were at their
727 maximum extension. Although the model NINO3 anomaly was rising during the termination,
728 the ITCZ was still closer to its southernmost position during the late Pleistocene (cf. Broccoli et
729 al., 2006), making the source of moisture too distant to be advected to North America either in
730 winter into the westerly flow by an enlarged Aleutian Low (cf. Santa Barbara Basin data by
731 Grelaud et al., 2009), or in summer, when initiation of tropical cyclone circulation would be
732 affected negatively by the reduced Coriolis force as the region of atmospheric instability lies
733 closer to the Equator.

734

735 6.3. Implications on hydroclimate analysis of southwestern North America

736 Our results indicate that tropical cyclones constitute a relevant player along with winter
737 extratropical cyclones and the NAM in late Pleistocene hydroclimatology of the southwestern
738 continent. The arrival of tropical moisture is therefore not only tied to sourcing flooding events
739 that help maintain high lake levels, as suggested by Lyle et al. (2012), but also to major sediment
740 transport events affecting both the arid and semiarid catchments of the region and the lowlands.
741 In our study, direct summer high intensity, relatively long-lived, and widespread storms affected
742 the southern Baja California region, and could spread north as far as 25 N and beyond given
743 ocean conditions recorded at that latitude for at least the late Pleistocene-Holocene transition (cf.
744 Lyle et al., 2010; Rodriguez-Sanz et al., 2013). More research is warranted, especially focusing
745 in the areas north of our study sites in southern California that show similar timing to our record,
746 as discussed above, but that have been interpreted as derived from other synoptic patterns. In
747 addressing this problem, detailed attention must be put into describing and interpreting the
748 sedimentology of the deposits, as it has proven critical in our research to understand storm
749 conditions that generate the alluvial deposits.

750 A direct outcome for future research will be the improved understanding of climate
751 conditions and landscape variables governing the arrival of powerful tropical storms to the
752 continent. This in turn will help all involved scientific and broader communities to better assess
753 and prepare for current and future unique related hazards. A recent analysis has shown for
754 example that the largest variability in summer precipitation during the 20th century in southern
755 California is explained by tropical cyclone events (Fierro, 2014), not by ENSO or any other
756 forcing. This observation, coupled with predicted trends of intensification of tropical cyclones
757 worldwide for the 21st century (e.g., Emanuel, 2013), and to the results presented here, should
758 make the case to fully incorporate tropical cyclones into an integrated hazards approach for the
759 southwestern continent.

760

761 7. Conclusion

762 The alluvial sequence developed in southern Baja California represents regional, discrete
763 periods during the late Pleistocene and early Holocene when climatic conditions allowed more
764 and more intense tropical cyclone events to approach the peninsula generating large fluvial
765 discharges and pronounced aggradation of the alluvial fans. The linkage between tropical
766 cyclone precipitation and alluvial aggradation is supported by analysis of the sedimentology of

767 historical alluvial terraces which were deposited by large tropical cyclone events.
768 Sedimentological features linked to this deposition include horizontal planar bedding and the
769 generation and preservation of antidune bedforms, and coincide with features observed in older
770 units. Some geological features nevertheless are unique (i.e., transverse ribs, longer wavelength
771 antidunes) and reveal the extraordinary power of the storms that generated them.

772 A period of regional aggradation began near ~70 ka with the deposition of unit Qt2,
773 culminating at ~10 ka, with deposition of the alluvial unit Qt4 (Fig. 9). The thickest alluvial
774 deposits correspond to those of unit Qt2, followed by Qt3 and Qt4. A second, incisional phase
775 developed as regional incision of older units increased after deposition of unit Qt4, leading to the
776 progressive development of a channelized alluvial landscape and deposition of units Qt5 and Qt6
777 on it. Sedimentary packages in all units are composed of multiple 1-3 m thick alluvial packages
778 representing individual storms that deposited sediments in upper-flow stage beds. Aggradational
779 units (Qt2-Qt4) covered broad (>2 km) channels in the form of sheetflood deposition while
780 incisional stage deposits are mostly confined to channels of ~0.5-2 km width. Continuous
781 deposition of the thicker sequences at timescales of centuries to millennia is demonstrated by
782 closely spaced dates in vertical profiles. Disconformities between major units are evident,
783 indicated by partly eroded buried soils, and supporting the existence of discrete periods of
784 deposition.

785 The discrete depositional periods indicated by the chronological and stratigraphic
786 relations can be associated with specific periods when summer (JJAS) insolation in the eastern
787 Pacific at 10-20 N recorded maxima determined by precessional cycles. Modulation of this
788 pattern by El Niño-like conditions in the tropical Pacific is apparent, especially during the late
789 Pleistocene-Holocene transition, although more research is warranted to extend the range of
790 proxies that can be linked to this pattern into the Pleistocene.

791 A precession-controlled alluvial record for southern Baja California can be used as a
792 benchmark to discriminate tropically driven deposition in more complex alluvial records
793 elsewhere in southwestern North America. The late Pleistocene depositional series is mainly
794 comprised of three precession-cycled events (Fig. 9) followed by a reduction in size of units
795 during the Holocene. By comparing the chronology and sedimentology of the Baja California
796 alluvial fans to records in the Mojave and Sonoran deserts or along southern California (cf.

797 Owen et al., 2014), it should be possible to start differentiating between climate components,
798 even if winter-storm chronology partially overlaps with the tropically-driven series.

799

800 8. Acknowledgements

801 We thank two anonymous reviewers for their helpful comments on an earlier version of
802 our manuscript. U.S. National Science Foundation NSF EAR 1123481 grant to J.L.A., E.M., and
803 E.R. and US Army Research Office Contract No. DAAD19-03-1-0159 to E.M. supported this
804 research. J.L.A. was also funded by postdoctoral support funds from the Division of Earth and
805 Ecosystem Sciences (DEES) of the Desert Research Institute (DRI) and by the National
806 Research Center for Integrated Natural Disaster Management (Chile). L. Farfán and S. Mayer
807 (CICESE, Unidad La Paz) provided partial logistical support for field activities. Discussions with
808 G. Martinez (UABCS), K.-b. Liu (LSU), and A. Hidy (LLNL) improved the manuscript. S.
809 Baker (DRI) helped with figure design. G. Yang (Dalhousie) and E. Huenupi (DRI) performed
810 all analytical work for cosmogenic isotope extraction. This manuscript is contribution LLNL-
811 JRNL-676762.

812

813 9. References

- 814 Allen, J.R.L., 1982. *Sedimentary Structures: Their Character and Physical Basis*. Developments in Sedimentology,
815 30 (parts I and II). Amsterdam, Elsevier. 593 p.
- 816 Antinao, J.L., Farfán, L.M., 2013. Occurrence of landslides during the approach of tropical cyclone Juliette (2001)
817 into Baja California Sur, Mexico. *Atmosfera* 26 (2), 183-208.
- 818 Antinao, J.L., McDonald, E., 2011. Three Hundred Years of Hurricanes in Baja California from Documentary
819 Sources: Implications for Sediment Flux and Landscape Evolution in the Peninsula. Annual Conference,
820 56, American Association of Geographers, Seattle.
- 821 Armstrong, P., Perez, R., Owen, L.A., Finkel, R.C., 2010. Timing and controls on late Quaternary landscape
822 development along the eastern Sierra el Mayor, northern Baja California, Mexico. *Geomorphology* 114 (3),
823 415-430.
- 824 Arriaga-Ramírez, S., Cavazos, T., 2010. Regional trends of daily precipitation indices in northwest Mexico and
825 southwest United States. *Journal of Geophysical Research*, vol. 115, D14111, doi:10.1029/2009JD013248.
- 826 Balco G., Stone J., Lifton N., Dunai T., 2008. A simple, internally consistent, and easily accessible means of
827 calculating surface exposure ages and erosion rates from Be-10 and Al-26 measurements. *Quaternary*
828 *Geochronology* 3, pp. 174-195. doi: 10.1016/j.quageo.2007.12.001
- 829 Berger, A., Loutre, M., 1991. Insolation values for the climate of the last 10 million years. *Quaternary Science*
830 *Reviews* 10 (4), 297-317.

831 Blanchet, C.L., Thouveny, N., Vidal, L., Leduc, G., Tachikawa, K., Bard, E., Beaufort, L., 2007. Terrigenous input
832 response to glacial/interglacial climatic variations over southern Baja California: a rock magnetic approach.
833 *Quaternary Science Reviews* 26 (25-28), 3118-3133.

834 Blisniuk, K., Oskin, M., Fletcher, K., Rockwell, T., Sharp, W., 2012. Assessing the reliability of U-series and ¹⁰Be
835 dating techniques on alluvial fans in the Anza Borrego Desert, California. *Quaternary Geochronology* 13
836 (0), 26-41.

837 Blisniuk, K., Rockwell, T., Owen, L.A., Oskin, M., Lippincott, C., Caffee, M.W., Dortch, J., 2010. Late Quaternary
838 slip rate gradient defined using high-resolution topography and Be dating of offset landforms on the
839 southern San Jacinto fault zone, California. *Journal of Geophysical Research* 115 (B08401).
840 doi:10.1029/2009JB006346.

841 Bonillas, E., 1984. Análisis Hidrológico de la zona sur del estado de Baja California Sur. BSc Thesis, U. Sonora,
842 Mexico. 126 p.

843 Brocard, G., van der Beek, D., Bourlès, D., Siame, L., Mugnier, J.-, 2003. Long-term fluvial incision rates and
844 postglacial river relaxation time in the French Western Alps from ¹⁰Be dating of alluvial terraces with
845 assessment of inheritance, soil development and wind ablation effects. *Earth and Planetary Science Letters*
846 209, 197-214.

847 Broccoli, A.J., Dahl, K.A., Stouffer, R.J., 2006. Response of the ITCZ to Northern Hemisphere cooling.
848 *Geophysical Research Letters* 33 (1).

849 Brown, N.D., Rhodes, E.J., Antinao, J.L., McDonald, E.V., 2014. Single-grain post-IR IRSL signals from K-
850 feldspars from alluvial fan deposits in Baja California Sur, Mexico. *Quaternary International* 362: 132-138.
851 doi:10.1016/j.quaint.2014.10.024.

852 Bull, W.B., 1991. *Geomorphic responses to climatic change*. Oxford University Press, Oxford.

853 Busch, M.M., Arrowsmith, J.R., Umhoefer, P.J., Coyan, J.A., Maloney, S.J., Gutiérrez, G.M., 2011. Geometry and
854 evolution of rift-margin, normal-fault–bounded basins from gravity and geology, La Paz–Los Cabos region,
855 Baja California Sur, Mexico. *Lithosphere* 3 (2), 110-127.

856 Castro, C.L., McKee, T.B., Pielke, R.A., 2001. The Relationship of the North American Monsoon to Tropical and
857 North Pacific Sea Surface Temperatures as Revealed by Observational Analyses. *Journal of Climate* 14
858 (24), 4449-4473.

859 Cayan, D., Webb, R., 1992. El Niño/Southern Oscillation and streamflow in the western United States. In: Díaz,
860 H.F., Markgraf, V. (Eds.), *El Niño: Historical and paleoclimate aspects of the Southern Oscillation*.
861 Cambridge University Press, Cambridge, pp. 29-68.

862 Cayan, D.R., Redmond, K.T., Riddle, L.G., 1999. ENSO and hydrologic extremes in the Western United States.
863 *Journal of Climate*, 12(9), 2881-2893.

864 Chu, P., 2004. ENSO and Tropical Cyclone Activity. In: Murnane, R.J., Liu, K. (Eds.), *Hurricanes and Typhoons:
865 Past, Present, and Future*. Columbia University Press, pp. 297-332.

866 Clapp, E.M., Bierman, P.R., Nichols, K.K., Pavich, M., Caffee, M., 2001. Rates of sediment supply to arroyos from
867 upland erosion determined using in situ-produced cosmogenic ¹⁰Be and ²⁶Al. *Quaternary Research* 55,
868 235-245.

869 Clark, P.U., Dyke, A.S., Shakun, J.D., Carlson, A.E., Clark, J., Wohlfarth, B., Mitrovica, J.X., Hostetler, S.W.,
870 McCabe, 2009. The Last Glacial Maximum. *Science* 325, 710-714.

871 Clement, A.C., Seager, R., Cane, M.A., 1999. Orbital controls on the El Niño/Southern Oscillation and the tropical
872 climate. *Paleoceanography* 14 (4), 441-456.

873 Davis, L., 2003. Geoarchaeology and geochronology of pluvial Lake Chapala, Baja California, Mexico.
874 *Geoarcheology* 18 (2), 205-223.

875 Del Monte-Luna, P., Arreguín-Sánchez, F., Godínez-Orta, L., López-Ferreira, C.A., 2005. Batimetría actualizada
876 de la Bahía de La Paz, Baja California Sur, México. *Océánides* 20 (1-2), 75-77.

877 Díaz, S.C., Salinas-Zavala, C.A., Hernández-Vázquez, S., 2008. Variability of rainfall from tropical cyclones in
878 northwestern Mexico and its relation to SOI and PDO. *Atmósfera* 21 (2), 213-223.

879 Driscoll, R. S., Merkel, D.L., Radloff, D. L., Snyder, D.E., Hagihara, J.S., 1984. An ecological land classification
880 framework for the United States. U.S. Department of Agriculture, Miscellaneous Publication 1439,
881 Washington, DC, 56 pp.

882 Duller, R., Warner, N.H., De Angelis, S., Armitage, J.J., Poyatos-More, M., 2015. Reconstructing the timescale of a
883 catastrophic fan-forming event on Earth using a Mars model. *Geophysical Research Letters*. 42, 10,324–
884 10,332, doi:10.1002/2015GL066031.

885 Elsner, J.B., Kara, A.B., 1999. *Hurricanes of the North Atlantic: Climate and Society*. Oxford University Press. 488
886 p.

887 Emanuel, K.A., 2013. Downscaling CMIP5 climate models shows increased tropical cyclone activity over the 21st
888 century, *Proceedings of the National Academy of Sciences* 110 (30),: 12219-12224.

889 Englehart, P.J., Douglas, A.V., 2001. The role of eastern North Pacific tropical storms in the rainfall climatology of
890 western Mexico. *International Journal of Climatology* 21 (11), 1357-1370.

891 Etheredge, D., Gutzler, D.S., Pazzaglia, F.J., 2004. Geomorphic response to seasonal variations in rainfall in the
892 Southwest United States. *Geological Society of America Bulletin* 116, 606-618.

893 Farfán, L. M., 2004. Regional Observations during the Landfall of Tropical Cyclone Juliette (2001) in Baja
894 California, Mexico. *Monthly Weather Review*. 132, 1575-1589.

895 Farfán, L.M., Fogel, I., 2007. Influence of tropical cyclones on humidity patterns over southern Baja California,
896 Mexico. *Monthly Weather Review*, 135, 1208-1214.

897 Fierro, A. O., 2014. Relationships between California rainfall variability and large-scale climate drivers.
898 *International Journal of Climatology* 34, 3626–3640. doi:10.1002/joc.4112.

899 Fierstine, H.L., Applegate, S.P., González-Barba, G., Schwennicke, T., Espinosa-Arrubarrena, L., 2001. A fossil
900 blue marlin (*Makaira nigricans* Lacépède) from the Middle Facies of the Trinidad Formation (Upper
901 Miocene to Upper Pliocene), San José del Cabo Basin, Baja California Sur, México. *Bulletin of the*
902 *Southern California Academy of Sciences* 100, 59-73.

903 Fletcher, J.M., Mungui, L., 2000. Active continental rifting in southern Baja California, Mexico: Implications for
904 plate motion partitioning and the transition to seafloor spreading in the Gulf of California. *Tectonics* 19 (6),
905 1107-1123.

906 Foley, M.G., 1977. Gravel-lens formation in antidune regime flow—a quantitative hydrodynamic indicator. *Journal*
907 *of Sedimentary Petrology* 47(2), 738-746.

908 Forbis, T.D., Douglas, R., Gorsline, D., Nava-Sanchez, E., Mack, L., Banner, J., 2004. Late Pleistocene (Last
909 Interglacial) terrace deposits, Bahia Coyote, Baja California Sur, Mexico. *Quaternary International* 120 (1),
910 29-40.

911 Frankel, K.L., Brantley, K.S., Dolan, J.F., Finkel, R.C., Klinger, R.E., Knott, J.R., Machette, M.N., Owen, L.A.,
912 Phillips, F.M., Slate, J.L., 2007. Cosmogenic ¹⁰Be and ³⁶Cl geochronology of offset alluvial fans along
913 the northern Death Valley fault zone; implications for transient strain in the eastern California shear zone.
914 *Journal of Geophysical Research* 112, B06407.

915 Frankel, K.L., Brantley, K.S., Dolan, J.F., Finkel, R.C., Klinger, R.E., Knott, J.R., Machette, M.N., Owen, L.A.,
916 Phillips, F.M., Slate, J.L., 2007. Cosmogenic ¹⁰Be and ³⁶Cl geochronology of offset alluvial fans along
917 the northern Death Valley fault zone; implications for transient strain in the eastern California shear zone.
918 *Journal of Geophysical Research* 112, B06407.

919 Gochis, D.J., Berberry, E.H., 2011. Contributions from the North American Monsoon Experiment towards improved
920 understanding and prediction of high impact weather and climate events. In: Chang, C., Ding, Y., Lau, N.,
921 Johnson, R.H., Wang, B., Yasunari, T. (Eds.), *The Global Monsoon System*. World Scientific, Singapore,
922 pp. 159-180.

923 Gochis, D.J., Brito-Castillo, L., James Shuttleworth, W., 2007. Correlations between sea-surface temperatures and
924 warm season streamflow in northwest Mexico. *International Journal of Climatology* 27 (7), 883-901.

925 Gosse, J.C., Phillips, F.M., 2001. Terrestrial in situ cosmogenic nuclides; theory and application. *Quaternary*
926 *Science Reviews* 20 (14), 1475-1560.

927 Gray, W.M., Sheaffer, J.D., 1991. El Niño and QBO influences on tropical cyclone activity. In: Glantz, M.H., Katz,
928 R.W., Nicholls, N. (Eds.), *Teleconnections linking worldwide anomalies*. Cambridge University Press,
929 Cambridge, pp. 257-284.

930 Grelaud, M., Beaufort, L., Cuven, S., Buchet, N., 2009. Glacial to interglacial primary production and El Niño–
931 Southern Oscillation dynamics inferred from coccolithophores of the Santa Barbara Basin.
932 *Paleoceanography* 24, PA1203.

933 Gutzler, D., 2004. An index of interannual precipitation variability in the core of the North American monsoon
934 region. *Journal of Climate* 17 (22), 4473-4480.

935 Haug, G.H., Hughen, K.A., Sigman, D.M., Peterson, L.C., Rohl, U., 2001. Southward Migration of the Intertropical
936 Convergence Zone Through the Holocene. *Science* 293 (5533), 1304-1308.

937 Hidy, A., Gosse, J.C., Blum, M.D., Gibling, M.R., 2014. Glacial–interglacial variation in denudation rates from
938 interior Texas, USA, established with cosmogenic nuclides. *Earth and Planetary Science Letters* 390, 209-
939 221. <http://dx.doi.org/10.1016/j.epsl.2014.01.011>.

940 Hidy, A.J., Gosse, J.C., Pederson, J.L., Mattern, J.P., Finkel, R.C., 2010. A geologically constrained Monte Carlo
941 approach to modeling exposure ages from profiles of cosmogenic nuclides: An example from Lees Ferry,
942 Arizona. *Geochemistry, Geophysics, Geosystems* 11, Q0AA10.

943 Hua, Q., Barbetti, M., Rakowski, A., 2013. Atmospheric Radiocarbon for the Period 1950–2010. *Radiocarbon*,
944 55(4), 2059-2072. doi:10.2458/azu_js_rc.55.16177.

945 Huckleberry, G., 1996. Historical Geomorphology of the Gila River. Arizona Geological Survey Open-File Report
946 96-14, 31 pp.

947 Huntley, D.J., Lamothe, M., 2001. Ubiquity of anomalous fading in Kfeldspars and the measurement and correct.
948 *Canadian Journal of Earth Sciences* 38, 1093-1106.

949 Jáuregui, E., 2003. Climatology of landfalling hurricanes and tropical storms in Mexico. *Atmósfera* 16, 193–204.

950 Jien, J.Y., Gough, W.A., Butler, K., 2015. The influence of El Niño-Southern Oscillation on tropical cyclone
951 activity in the Eastern North Pacific Basin. *Journal of Climate* 28, 2459–2474.

952 Kennedy, J. F., 1961. Stationary waves and antidunes in alluvial channels: Report No. KH-R-2, W. M. Keck
953 Laboratory of Hydraulics and Water Resources, California Institute of Technology, Pasadena, Calif., 146 p.

954 Kennedy, J.F., 1969. The formation of sediment ripples, dunes and antidunes. *Annual Reviews of fluid Mechanics*,
955 1, 147-168.

956 Kent, E.J., 2011. Towards defining the extent of climatic influence on alluvial fan sedimentation in semi-arid
957 Sonoran and Mojave Deserts, southern California, USA and Baja California, northern Mexico. MSc Thesis,
958 U. Cincinatti, Ohio, 53 p.

959 Kirby, M.E., Feakins, S.J., Bonuso, N., Fantozzi, J.M., Hiner, C.A., 2013. Latest Pleistocene to Holocene
960 hydroclimates from Lake Elsinore, California. *Quaternary Science Reviews* 76 (0), 1-15.

961 Kirby, M.E., Lund, S.P., Bird, B.W., 2006. Mid-Wisconsin sediment record from Baldwin Lake reveals hemispheric
962 climate dynamics (Southern CA, USA). *Palaeogeography, Palaeoclimatology, Palaeoecology* 241 (2), 267-
963 283.

964 Kirby, M.E., Zimmerman, S.R.H., Patterson, W.P., Rivera, J.J., 2012. A 9170-year record of decadal-to-multi-
965 centennial scale pluvial episodes from the coastal Southwest United States: a role for atmospheric rivers?
966 *Quaternary Science Reviews* 46 (0), 57-65.

967 Koutavas, A., Joanides, S., 2012, El Niño–Southern Oscillation extrema in the Holocene and Last Glacial
968 Maximum, *Paleoceanography*, 27, PA4208, doi:10.1029/2012PA002378.

969 Koutavas, A., Lynch-Stieglitz, J., 2005. Variability of the Marine ITCZ over the eastern Pacific during the past
970 30,000 years. In: Diaz, H.F., Bradley, R.S. (Eds.), *The Hadley Circulation: Present, Past and Future*.
971 Kluwer Academic Publishers, Dordrecht, pp. 347-369.

972 Koutavas, A., Lynch-Stieglitz, J., Marchitto Jr., T.M., Sachs, J.P., 2002. El Niño–Like Pattern in Ice Age Tropical
973 Pacific Sea Surface Temperature. *Science* 297 (5579), 226-230.

974 Leckie, D.A., 1994. Canterbury Plains, New Zealand — implications for sequence stratigraphic models, *American*
975 *Association of Petroleum Geologists Bulletin* 78, 1240–1256.

976 Li, H.-., Xu, X.-., Ku, T.-., You, C.-., Buchheim, H.P., Peters, R., 2008. Isotopic and geochemical evidence of
977 palaeoclimate changes in Salton Basin, California, during the past 20 kyr: 1. $\delta^{18}O$ and $\delta^{13}C$ records in lake
978 tufa deposits. *Palaeogeography Palaeoclimatology Palaeoecology* 259 (2-3), 182-197.

979 Lozano-García, M.S., Ortega Guerrero, B., Sosa-Najera, S., 2002. Mid- to Late-Wisconsin Pollen Record of San
980 Felipe Basin, Baja California. *Quaternary Research* 58 (1), 84-92.

981 Lyle, M., Heusser, L., Ravelo, C., Andreasen, D., Olivarez Lyle, A., Diffenbaugh, N., 2010. Pleistocene water cycle
982 and eastern boundary current processes along the California continental margin, *Paleoceanography*, 25,
983 PA4211, doi:10.1029/2009PA001836.

984 Lyle, M., Heusser, L., Ravelo, C., Yamamoto, M., Barron, J.A., Diffenbaugh, N.S., Herbert, T., Andreasen, D.,
985 2012. Out of the Tropics: The Pacific, Great Basin Lakes, and Late Pleistocene Water Cycle in the Western
986 United States. *Science* 337, 1629-1633. doi: 10.1126/science.1218390.

987 Mahan, S.A., Miller, D.M., Menges, C.M., Yount, J.C., 2007. Late Quaternary stratigraphy and luminescence
988 geochronology of the northeastern Mojave Desert. *Quaternary International* 166 (1), 61-78.

989 Maloney, S.J., 2009. Late Quaternary Faulting History of the Northern El Carrizal Fault, Baja California Sur,
990 Mexico. Master or Science, Geology Thesis, Northern Arizona University, Flagstaff, 196 pp.

991 Martinez Gutierrez, G., Mayer, L., 2004. Huracanes en Baja California, México, y sus implicaciones en la
992 sedimentación en el Golfo de California. *GEOS* 24(1), 57-64.

993 Martínez-Gutiérrez, G., Sethi, P.S., 1997. Miocene-Pleistocene sediments within the San José del Cabo Basin, Baja
994 California Sur, Mexico. *Geological Society of America Special Papers* 318, 141-166.

995 Masters, P., 2006. Holocene sand beaches of southern California: ENSO forcing and coastal processes on millennial
996 scales. *Palaeogeography, Palaeoclimatology, Palaeoecology* 232 (1), 73-95.

997 Matmon, A., Schwartz, D.P., Finkel, R., Clemmens, S., Hanks, T., 2005. Dating offset fans along the Mojave
998 section of the San Andreas fault using cosmogenic ^{26}Al and ^{10}Be . *Geological Society of America Bulletin*,
999 117, 5-6, 795-807.

1000 McGill, S.F., Owen, L.A., Weldon, R.J., Kendrick, K.J., 2013. Latest Pleistocene and Holocene slip rate for the San
1001 Bernardino strand of the San Andreas fault, Plunge Creek, Southern California: Implications for strain
1002 partitioning within the southern San Andreas fault system for the last ~35 k.y. *Geological Society of
1003 America Bulletin* 125 (1-2), 48-72.

1004 Metcalfe, S., Say, A., Black, S., McCulloch, R., O'Hara, S., 2002. Wet Conditions during the Last Glaciation in the
1005 Chihuahuan Desert, Alta Babicora Basin, Mexico. *Quaternary Research* 57 (1), 91-101.

1006 Miall, A., 1996. *The geology of fluvial deposits: sedimentary facies, basin analysis, and petroleum geology.*
1007 Springer, Berlin.

1008 Miall, A., 2000. *Principles of sedimentary basin analysis.* Springer, Berlin.

1009 Miller, D.M., Schmidt, K.M., Mahan, S.A., McGeehin, J.P., Owen, L.A., Barron, J.A., Lehmkuhl, F., Lohrer, R.,
1010 2010. Holocene landscape response to seasonality of storms in the Mojave Desert. *Quaternary International*
1011 215 (1-2), 45-61.

1012 Owen, L.A., Clemmens, S.J., Finkel, R.C., Gray, H., 2014. Late Quaternary alluvial fans at the eastern end of the
1013 San Bernardino Mountains, Southern California. *Quaternary Science Reviews* 87, 114-134.

1014 Parker, J.T.C., 1995. Channel Change and Sediment Transport in Two Desert Streams in Central Arizona, 1991-92.
1015 U.S. Geological Survey Water-Resources Investigations Report 95-4059, 42 pp.

1016 Raga, G.B., Bracamontes-Cevallos, B., Farfán, L.M., Romero-Centeno, R., 2013. Landfalling tropical cyclones on
1017 the Pacific coast of Mexico: 1850-2010. *Atmósfera* 26(2), 209-220.

1018 Reimer, P., Bard, E., Bayliss, A., Beck, J., Blackwell, P., Bronk Ramsey, C., Buck, C., Cheng, H., Edwards, R.,
1019 Friedrich, M., Grootes, P., Guilderson, T., Haflidason, H., Hajdas, I., Hatté, C., Heaton, T., Hoffmann, D.,
1020 Hogg, A., Hughen, K., Kaiser, K., Kromer, B., Manning, S., Niu, M., Reimer, R., Richards, D., Scott, E.,
1021 Southon, J., Staff, R., Turney, C., van der Plicht, J., 2013. IntCal13 and Marine13 Radiocarbon Age
1022 Calibration Curves 0–50,000 Years cal BP. *Radiocarbon*, 55(4), 1869-1887.
1023 doi:10.2458/azu_js_rc.55.16947.

1024 Rhode, D., 2002. Early Holocene juniper woodland and chaparral taxa in the Central Baja California peninsula,
1025 Mexico. *Quaternary Research* 57 (1), 102-108.

1026 Rhodes, E.J., 2011. Optically Stimulated Luminescence Dating of Sediments over the Past 200,000 Years. *Annual*
1027 *Review of Earth and Planetary Sciences* 39, 461-488.

1028 Robert, C., 2004. Late Quaternary variability of precipitation in Southern California and climatic implications: clay
1029 mineral evidence from the Santa Barbara Basin, ODP Site 893. *Quaternary Science Reviews* 23 (9-10),
1030 1029-1040.

1031 Rodgers, E.B., Adler, R.F., Pierce, H.F., 2000. Contribution of tropical cyclones to the North Pacific climatological
1032 rainfall as observed from satellites. *Journal of Applied Meteorology* 39, 1658–1678.

1033 Rodríguez-Sanz, L., Mortyn, P. G. , Herguera, J. C. , Zahn, R., 2013. Hydrographic changes in the tropical and
1034 extratropical Pacific during the last deglaciation, *Paleoceanography*, 28, 529–538, doi:10.1002/palo.20049.

1035 Romero-Vadillo, E., Zaytsev, O., Morales-Pérez, R. 2013. Tropical cyclone statistics in the northeastern Pacific,
1036 *Atmosfera*, 20, 197–213.

1037 Roy, P.D., Caballero, M., Lozano, S., Morton, O., Lozano, R., Jonathan, M.P., Sánchez, J.L., Macías, M.C. , 2012.
1038 Provenance of sediments deposited at paleolake San Felipe, western Sonora Desert: Implications to regimes
1039 of summer and winter precipitation during last 50 cal kyr BP, *Journal of Arid Environments*, 81, 47-58, doi:
1040 10.1016/j.jaridenv.2012.01.008.

1041 Roy, P.D., Quiroz-Jiménez, J.D., Chávez-Lara, C.M., Sánchez-Zavala, J.L., Pérez-Cruz, L.L., Sankar, G.M., 2014.
1042 Humid Pleistocene–Holocene transition and early Holocene in sub-tropical northern Mexico and possible
1043 Gulf of California forcing. *Boreas* 43 (3), 577-587.

1044 Roy, P.D., Quiroz-Jiménez, J.D., Pérez-Cruz, L.L., Lozano-García, S., Metcalfe, S.E., Lozano-Santacruz, R., López-
1045 Balbiaux, N., Sánchez-Zavala, J.L., Romero, F.M., 2013. Late Quaternary paleohydrological conditions in
1046 the drylands of northern Mexico: a summer precipitation proxy record of the last 80 cal ka BP. *Quaternary*
1047 *Science Reviews* 78 (0), 342-354.

- 1048 Sirkin, L., Pedrín-Avilés, S., Padilla-Arredondo, G., Díaz-Rivera, E., 1994. Holocene vegetation and climate of Baja
1049 California Sur, Mexico. *Revista Mexicana de Ciencias Geológicas* 11 (1), 79-86.
- 1050 Spelz, R.M., Fletcher, J.M., Owen, L.A., Caffee, M.W., 2008. Quaternary alluvial-fan development, climate and
1051 morphologic dating of fault scarps in Laguna Salada, Baja California, Mexico. *Geomorphology* 102 (3-4),
1052 578-594.
- 1053 Staines-Urias, F., González-Yajimovich, O., Beaufort, L., 2015. Reconstruction of past climate variability and
1054 ENSO-like fluctuations in the southern Gulf of California (Alfonso Basin) since the last glacial maximum,
1055 *Quaternary Research* 83(3), 488-501. <http://dx.doi.org/10.1016/j.yqres.2015.03.007>.
- 1056 Summerfield, M.A., 1985. Plate tectonics and landscape development on the African continent. In: Morisawa, M.,
1057 Hack, J., Editors, *Tectonic Geomorphology*, Allen and Unwin, Boston, pp. 27–51.
- 1058 Szabo, B.J., Hausback, B.P., Smith, J.T., 1990. Relative inactivity during the last 140,000 years of a portion of the
1059 La Paz fault, southern Baja California Sur, Mexico. *Environmental Geology and Water Sciences* 15 (2),
1060 119-122.
- 1061 Umhoefer, P.J., Maloney, S.J., Buchanan, B., Arrowsmith, J.R., Martinez-Gutiérrez, G., Kent, G., Driscoll, N.,
1062 Harding, A., Kaufman, D., Rittenour, T., 2014. Late Quaternary faulting history of the Carrizal and related
1063 faults, La Paz region, Baja California Sur, Mexico. *Geosphere* 10 (3), 476-504.
- 1064 van der Woerd, J., Klinger, Y., Sieh, K., Tapponnier, P., Ryerson, F.J., Mériaux, A.-S., 2006. Long-term slip rate
1065 of the southern San Andreas fault from ¹⁰Be-²⁶Al surface exposure dating of an offset alluvial fan. *Journal*
1066 *of Geophysical Research* 111 (B04407). doi:10.1029/2004JB003559.
- 1067 Van Devender, T.R., 1997. 21,000 years of vegetation change in the northern Vizcaino, Baja California. Second
1068 Annual Baja California Botanical Symposium, August 14-16, 1997, San Diego, California.
- 1069 Villanueva, E., 2001. Presencia de Huracanes en Baja California Sur. El caso del ciclón Liza. Tesis Maestro Historia
1070 Regional, Universidad Autónoma Baja California Sur, La Paz, Baja California Sur, México, 279 pp.
- 1071 Wagner, J.D.M., Cole, J.E., Beck, J.W., Patchett, P.J., Henderson, G.M., Barnett, H.R., 2010. Moisture variability in
1072 the southwestern United States linked to abrupt glacial climate change. *Nature Geoscience* 3 (2), 110-113.
- 1073 Webb, R.H., Magirl, C.S., Griffiths, P.G., Boyer, D.E., 2008. Debris flows and floods in the southeastern Arizona
1074 from extreme precipitation in July 2006: Magnitude, frequency, and sediment delivery. U.S. Geological
1075 Survey Open File Report 2008-1274, 95 pp.
- 1076 Wintle, A.G., Murray, A.S., 2006. A review of quartz optically stimulated luminescence characteristics and their
1077 relevance in single-aliquot regeneration dating protocols. *Radiation Measurements* 41, 369-391.
- 1078
- 1079
- 1080 Figure captions
- 1081 Figure 1. Study area and regional context. Location of Figures 2A, 2B is shown. Note location of studied basins and
1082 major cities mentioned in text. The normal faults and faults with potential normal or strike-slip movement
1083 (stippled) defining the basins are also shown. Inset shows moisture source pathways towards southwestern
1084 North America from the Pacific Ocean: extratropical cyclones, EC, stippled; enhanced water vapor (EWV)

1085 bands, solid line; East Pacific tropical cyclones (TC), with typical trajectories, including recurving cyclone
1086 trajectories, solid lines, and the North American Monsoon (NAM, moisture trajectories shown with stippled
1087 arrows). The Sonoran Desert is highlighted in the inset, along with the Mojave (M) and Chihuahuan (C)
1088 deserts. 1: ODP893 core location; 2: MD02-2508 core location.

1089

1090 Figure 2. Map depicting extension of units and geochronology sampling sites, with selected ages. Location of
1091 sections described in the text, cosmogenic depth profiles and soil pits is also shown. A. San José basin; B.
1092 La Paz basin. C. Stratigraphic section between Caduaño and Santa Rosa (section JK). Note summary age
1093 ranges for units. Projected bed level for Arroyo San José is shown to give an idea of local base level for
1094 each stream. Distance from the place of section to Arroyo San José is 5-8 km.

1095 Figure 3. Field photographs of units Qt1 and Qt2. A. Lower portion of Qt1 unit covered with beach deposits in east
1096 Coyote Bay; the section exposes 2 m of a Bt horizon developed mostly in beach gravels, below it ~1m of
1097 Bk horizon overlying ~10 m of boulders and gravels. B. Qt1 unit sediments exposed along a section of
1098 route 1 at Arroyo Hondo (La Paz). The Bt horizon has been truncated by erosion, especially towards the
1099 south (right) of the section. The white accumulation on surfaces near the top 1-2 m corresponds to a
1100 siliceous duripan (Bqm horizon). C. West Coyote Bay Qt1 pit (REC-1); note depth of Bt horizon, and
1101 below it Bk horizon. The whole section is stratigraphically on top of the beach deposits in Fig. 3A. D. View
1102 of Qt2 unit in Caduaño (San José basin). Note the deep (~3-5 m) B horizon. Cerro Guayparin Grande is
1103 shown to highlight the topographic relief in this region. E. Photomosaic of section by Arroyo El Salto (La
1104 Paz basin). Qt2 sediments below what it appears to be Qt3 sediments. Note to the right the relatively
1105 younger sediment infill (Qt5? based on soil development) of a channel, with interpreted flow perpendicular
1106 and away from the section, very similar to present-day flow in the modern channel.

1107 Figure 4. Sedimentological sections in units Qt2 and Qt3 in San José Basin. Upper panel. San Lazaro III Section
1108 (Qt3; San José basin; Fig. 2); simplified boundaries of major depositional units is marked in red. In the
1109 inset, a sketch of the same units that highlights bedform dimensions. Average wavelength of the antidune
1110 bedforms in units A and B of the inset (15-20 m) is used to calculate mean flow depth and flow discharge
1111 (Table S-3; Supplementary Dataset) based on equations developed by Kennedy (1961). Note IRSL
1112 geochronology samples in the left portion of the section. Middle left panel: photomosaic of Encinal II
1113 section (Qt2; north San José basin, Fig. 2). Lower Panel: Encinal II interpreted section, symbols similar
1114 than upper panel.

1115 Figure 5. Cosmogenic depth profiles in Qt2 and Qt3 units in La Paz basin. A/E. Field photographs of pit sections
1116 displaying soil horizonation. IRSL ages in A and E (in ka) are used for comparison with depth profile
1117 results. B/F. Soil density variation with depth. C/G. Measured ^{10}Be concentration (black circles), and
1118 model ^{10}Be concentration with depth; gray curves are individual Montecarlo simulations; red curve is best-
1119 fit. D/H. Probability density functions for age and inheritance based on Bayesian analysis of simulation
1120 results (Hidy et al., 2010); minimum chi-square curves are also depicted.

1121 Figure 6. Field photographs of units Qt3 and Qt4. All IRSL ages shown in ka BP. A. Section by Arroyo La Palma
1122 (San José), exposing stacked Qt3 sediment packages, partially separated by subtle oxidized layers that do
1123 not show a well-developed soil structure, suggesting brief non-depositional periods. B. San Lázaro SLVIII
1124 section, where the contact between Qt3 and Qt4 units in San Jose basin is best expressed. To the east, the
1125 contact becomes difficult to follow, and mostly Qt3 sediments outcrop (e.g., in SL-III section, Fig. 4, about
1126 500 m east). To the southeast, on the terrace developed by the upper unit and ~1km to the southeast, pit SJ1
1127 was excavated (Fig. 6C). C. San Jose Airport Terrace Qt4 SJ-1 pit. Soil development is restricted compared
1128 to Qt3 and older units. D. San Jose Airport Terrace Qt4 SJ-2 pit. IRSL dating between 20.0 and 3.0 ka
1129 suggests bioturbation rather than redeposition, consistent with soil development and lack of obvious
1130 sedimentology features up to 1.8m deep. E. Spatial relation between Qt5 and Qt4 units in Cajoncito, La
1131 Paz. IRSL ages are shown in the section.

1132 Figure 7. Field photographs of unit Qt5. A. Santa Anita (Qt4) terrace to the left, incised by present-day channel, with
1133 Qt5 (cultivated) terrace about 500 m wide. Height of Qt5 terrace is about 3 m above the modern channel
1134 with Qt6 deposits (far right, sparse vegetation). B. San José Airport terrace (Qt4) to the right, incised by
1135 present-day channel, with Qt5 (vegetated) terraces 0.5-1 km wide. Height of Qt5 terrace is about 3 m above
1136 the modern channel and bar deposits (with sparse vegetation). Note location of sampling sections SL-1 (in
1137 channel, Qt6, ~0.4 ka), and SL-4 (Qt5, 3 m above channel, 0.4-0.5 ka). C. Qt5 sediments near Los Arquitos
1138 (La Paz basin), in a natural section exposed by action of present-day channel erosion. Shovel is about 0.5 m
1139 high. Flow towards the right. Note downstream dipping cross-bedding along with horizontal bedding at top
1140 and bottom. D. Qt5 terrace near Mesquitito (La Paz basin), eroded actively by present-day channel, Qt5
1141 surface ~ 2.6 m above it. The upper ~1.7 m of the deposit has been partially bioturbated, suggested by the
1142 1802-1938 AD and post-1950 AD ages found in charred material at 0.8 and 1.7 m from the surface (Table
1143 3), and the weak soil developed on it. E. Detailed soil profile for Mesquitito site, showing the sequence of
1144 ages and interpreted units. The preferred age of the upper deposit (Qt5o) is marked by the 4790 ± 40 cal BP
1145 marine bivalve shell found at 1.0 m, probably incorporated from a midden upstream, and matching the
1146 IRSL age of 6.0 ± 1.3 ka. Below the truncated buried soil, an IRSL age of 9.9 ± 2.7 ka marks unit Qt4.

1147 Figure 8. Field photographs and sedimentological section of unit Qt6 in La Paz (Cajoncito I section). A.
1148 Sedimentological features; note the low-angle upstream dipping beds interbedded with horizontal plane
1149 upper stage bedding, and partially preserved antidune bedforms (e.g., horizons A and B) with wavelengths
1150 up to 10-13 m. These measurements along with channel dimensions observed for this event (Villanueva,
1151 2001) were used to estimate the peak discharge for this storm (Table S-3; Supplementary Dataset). B. Field
1152 photograph of section shown in A (Cajoncito Qt6 terrace, mostly built during 1976 storm Liza) to the left,
1153 incised by present-day channel. C. IRSL ages for 1976 hurricane Liza deposit. IRSL dating is in agreement
1154 with bone dating (see D and Table 3), and the presence of artifacts in the layer down to 2.5 m. Mafic
1155 minerals dominate the dark layers on the upper portion of the deposit. D. Horizontal stratification is evident
1156 in this portion of the section. An oxidized piece of tin (can) crops ~0.8 m deep in the center of this

1157 photograph. A few meters east of here, down to a depth of 2.64 m, bone fragments were found and dated,
1158 with a maximum age of death of 1974 AD (Table 3).

1159 Figure 9. Alluvial fan chronology for Southern Baja California compared to paleoclimate proxies and climate
1160 forcing for southwestern North America. A. Santa Barbara ODP site 893 clay mineral assemblage used as a
1161 proxy for terrigenous discharge (Fig. 1; Robert, 2004). B. Lake records for Sonoran, southern California
1162 and Chihuahuan deserts (Kirby et al., 2006; Lozano-Garcia et al., 2002, Roy et al., 2012, 2014; Metcalfe et
1163 al., 2002) C. Alluvial chronology data for the westernmost Mojave and NW Sonoran deserts, organized
1164 according to latitude (on the left); cosmogenic depth profiles marked with squares (e.g., Blisniuk et al.,
1165 2010, 2012); individual boulder ages marked with circles (Frankel et al., 2007; Matmon et al., 2005; Spelz
1166 et al., 2008; van der Woerd et al., 2006; Kent, 2011). D. Magnetic stratigraphy in core MD02-2508
1167 offshore Baja California (Fig. 1), used as a proxy for terrigenous discharge (Blanchet et al., 2007). E.
1168 Summer (JJAS) insolation, 10-20 N (Berger, 1991). F. Grouped SBC chronology. Units marked by colors;
1169 cosmogenic depth profiles in square symbols, IRSL data in circles. Groupings for units Qt2, 3, and 4
1170 defined broadly by the kernel density plot shown are displayed throughout the figure as gray bands. Note
1171 that open circles refer to IRSL ages that are inconsistent with soils data; these ages probably underestimate
1172 the age of unit and reflect bioturbation (see text for details). G. Modeled NINO3 SST anomaly (Clement et
1173 al., 1999). Last Glacial maximum (LGM) as in Clark et al. (2009), represented throughout the figure as a
1174 dark gray band.

1175
1176
1177
1178

Table 1. A. Summary of deposit thickness, surface morphology and soil morphology for the alluvial units.

Unit	Observed thickness (m)	Surface Morphology	Number of soil profiles	Soil Depth ¹ (cm)	B Thickness ² (cm)	B horizon Hue ³	B Horizon Type ⁴	Best Soil Structure ⁵	Dry Consistence ⁶	Finest Soil Texture
Qt6	2-3	Bar/swale	1	4	0	10YR	none	pl-sg	lo-so	S
Qt5y	2-3	Bar/swale	4	43-57	29-42	10YR	weak Bw	sg-sbk	so-sh	S
Qt5o	3-5	Flat	6	90-146	52-93	10YR	mod Bw	sbk	so-sh	LS
Qt4	5-10	Flat	4	286-291	181-246	10-8.75YR	strong Bw-weak Bt	sbk	so-sh	LS
Qt3	20-40	Flat	5	240-329	211-249	8.75-7.5YR	mod Bt	pr-sbk	sh-h	SL
Qt2	30-50	Ballena topography	2	287-290	190-210	2.5YR	strong Bt	pr-abk	h-vh	SCL
Qt1	~15- >20	Ballena topography, flat surfaces	1	326	278	5YR	strong Bt strong Bk ⁸	pr-abk	h-vh	CL

1: Total depth to top of first C horizon, minimum-maximum range where more than one soil

2: Thickness of B horizon (includes BC horizons), minimum-maximum range where more than one soil

3: Most rubified B horizon Munsell soil color hue

4: Best developed type of genetic B horizon (w = structure/color, t = accumulation of clay, k = accumulation of carbonate); mod = moderate.

5: Best developed type of soil structure (sg = single grain, pl = platy, sbk = subangular blocky, abk = angular blocky, pr = prismatic)

6: Strongest soil consistence: lo = loose, so= soft, sh = slightly hard, h = hard, vh = very hard

7: Finest soil texture (i.e. highest concentration of silt and clay) S = sand, LS = loamy sand, L = loam, SCL = sandy-clay loam, CL = clay loam.

8: All soils except the single soil described on the Qt1 lack pedogenic carbonate; the source of carbonate in the Qt1 soil is due to in-situ medication of marine coral deposits as the base of the soil.

Table 1. B. Summary of catchment bedrock, sedimentological properties and the interpreted sedimentary regime for each unit.

Unit	Catchment bedrock	Most common bedforms	Interpreted sedimentation regime
Qt6	Gneiss and granodiorites (SJ*), granites (LP*)	Horizontal planar, low angle cross bedding	Channelized flow
Qt5y	Gneiss and granodiorites (SJ), granites (LP)	Horizontal planar, low angle cross bedding	Upper regime flow, channelized flow
Qt5o	Gneiss and granodiorites (SJ),	Horizontal planar, low angle cross bedding	Upper regime flow
Qt4	Gneiss and granodiorites (SJ),	Horizontal planar, low angle cross bedding, antidunes	Upper regime flow
Qt3	Gneiss and granodiorites (SJ),	Antidunes, Horizontal planar, low angle cross bedding, transverse ribs (gravel bars)	Upper regime flow
Qt2	Gneiss and granodiorites (SJ),	Antidunes, Horizontal planar, low angle cross bedding, transverse ribs (gravel bars)	Upper regime flow
Qt1	Granites (LP south), volcaniclastics (LP north), gneisses (SJ)	Horizontal planar, low angle cross bedding,	Upper regime flow, channelized flow

(*) SJ: San José basin; LP: La Paz basin.

Table 2. Luminescence dating results. Ages reported here as in Brown et al. (2014), adding six new samples. Unit assignments are updated based on soils data for the pits and sections linked to the samples.

Site/Pit(†)	Lab ID*	Sample ID	Unit	Depth [m]	Age [ka] and uncertainty 1 s.d.
Qt6 unit (includes 1976 Liza deposit)					
Cajoncito north section, 1976 Liza on top (CAJ-I/II)	J0403	BA1205	1976	0.69	0.1 ± 0.1
	J0404	BA1206	1976	0.96	0.7 ± 0.5
	J0405	BA1207	1976	1.63	0.3 ± 0.1
	J0406	BA1208	1976	2.84	0.3 ± 0.1
San Lázaro channel, Qt6	J0425	BA1227	Qt6	0.47	0.4 ± 0.1
Arroyo San Lázaro, channel quarry, SL1	J0194	SL101	Qt6	0.8	0.4 ± 0.1
	J0195	SL102	Qt6	2.0	0.4 ± 0.1
Qt5 unit (includes Qt5y, Qt5o in Table 1, also Qt4 in lower portions of dated sections)					
Arroyo San Lázaro, section, SL4	J0200	SL401	Qt5	0.5	0.5 ± 0.1
	J0201	SL402	Qt5	0.9	0.4 ± 0.1
San Lázaro, section, 3 m terrace N side (by SL4)	J0423	BA1225	Qt5	0.75	0.5 ± 0.1
	J0424	BA1226	Qt5	0.75	0.3 ± 0.05
EAO-4 pit	J0129	EAO-04-L1	Qt5	1.50	3.3 ± 0.7
	J0130	EAO-04-L2	Qt5	1.70	2.4 ± 0.6
El Mesquitito shell site	J0415	BA1217	Qt5	1.17	6.0 ± 1.3
	J0416	BA1218	Qt4	1.95	9.9 ± 2.7
Bonfil bank, (same site as Maloney, 2009)	J0407	BA1209	Qt5	1.0	5.5 ± 0.8
	J0408	BA1210	Qt5	1.2	6.1 ± 1.3
	J0409	BA1211	Qt4	1.4	8.9 ± 1.2
	J0410	BA1212	Qt4	1.6	11.6 ± 2.1
Qt4 unit					
San José airport terrace, Pit SJ1	J0186	SJ101	Qt4	2.2	12.3 ± 1.1
	J0187	SJ102	Qt4	2.5	13.6 ± 1.2
	J0188	SJ103	Qt4	2.8	14.6 ± 1.3
	J0189	SJ104	Qt4	3.1	13.6 ± 1.2
San José airport terrace, Pit SJ2	J0190	SJ201	Qt4	0.9	3.0 ± 0.4

	J0191	SJ202	Qt4	1.4	4.6 ± 0.5
	J0192	SJ203	Qt4	2.0	7.0 ± 1.0
	J0193	SJ204	Qt4	2.8	20.4 ± 1.7
Santa Teresita terrace, Pit ST2	J0202	ST201	Qt4	0.7	1.0 ± 0.1
	J0203	ST202	Qt4	1.14	2.0 ± 0.2
	J0204	ST203	Qt4	1.6	4.8 ± 0.5
	J0205	ST204	Qt4	2.48	16.4 ± 2.8
Cajoncito south section (CAJ-III)	J0399	BA1201	Qt4	4.0	11.8 ± 2.2
	J0400	BA1202	Qt4	4.2	16.4 ± 2.9
	J0401	BA1203	Qt4	5.0	13.4 ± 3.1
Bonfil quarry, same site as Maloney (2009), upper section	J0412	BA1214	Qt4	2.60	20.7 ± 3.7
Qt3 unit					
Bonfil quarry, same site as Maloney (2009), lower section	J0413	BA1215	Qt3	0.40	34.6 ± 4.7
	J0414	BA1216	Qt3	1.08	30.4 ± 4.4
EAO-2 pit	J0127	EAO-02-L1	Qt3	2.15	31.0 ± 3.5
	J0128	EAO-02-L2	Qt3	1.70	26.4 ± 3.4
CAD-3 site	BAJA1	CAD3-1	Qt3	3.00	35.3 ± 1.9
Arroyo San Lázaro, section III (site SL3)	J0196	SL301	Qt3	15.0	30.6 ± 2.8
	J0197	SL302	Qt3	15.2	36.4 ± 3.6
	J0198	SL303	Qt3	15.4	36.1 ± 2.5
	J0199	SL304	Qt3	16.3	37.0 ± 2.9
Qt2 unit					
Ejido Alvaro Obregón (section below Qt3/Qt2 surface, by modern channel)	J0417	BA1219	Qt2	5.0	52.2 ± 4.8
	J0418	BA1220	Qt2	6.0	66.5 ± 6.8
Mesa del Moro terrace	J0419	BA1221	Qt2	5.0	58.8 ± 3.2
	J0420	BA1222	Qt2	5.0	55.7 ± 5.0
Desertica	J0421	BA1223	Qt2	1.8	62.7 ± 7.4
	J0422	BA1224	Qt2	1.8	65.0 ± 6.1
EAO-3 pit	BAJA3	EAO-07-JL1	Qt2	2.70	57.2 ± 4.4

†Sites in bold, San José basin.

* Samples J0127-0130 processed at UCLA, this study; samples BAJA1 and BAJA3 were processed and measured at DRI, this study. Samples J0186-J0424 processed and measured at UCLA and reported in Brown et al. (2014).

Table 3. Radiocarbon data.

Site/Pit	Lab Id, BETA	Sample ID and type	Unit	Depth [m]	Conventional age (BP, pMC) and uncertainty	$\delta^{13}\text{C}$	Calibrated age 2 sigma range and probability(*)
Cajoncito, Liza 1976	279501	CAJ003, bone	Qt6	1.61	160.9 ± 0.4 pMC	-18.3	[cal AD 1963.29 :cal AD 1963.35] 0.033 [cal AD 1966.95 :cal AD 1968.21] 0.866 [cal AD 1968.56 :cal AD 1968.71] 0.101
	279502	CAJ004, bone	Qt6	2.64	144.4 ± 0.5 pMC	-19.8	[cal AD 1962.80 :cal AD 1963.03] 0.128 [cal AD 1971.51 :cal AD 1971.55] 0.008 [cal AD 1972.26 :cal AD 1972.29] 0.003 [cal AD 1972.96 :cal AD 1974.88] 0.860
Mesquitito, shell site	279503	CAJ005, charred material	Qt5	0.77	90 ± 40	-28.3	[cal AD 1681- 1739] 0.278 [cal AD 1750- 1762] 0.018 [cal AD 1802- 1938] 0.704
	279504	CAJ006, shell	Qt5	1.00	4790 ± 40	+1.6	[cal BP 4596 – 4839] 1.000
	279505	CAJ007, charred material	Qt5	1.07	108.7 ± 0.4 pMC	-26.1	[cal AD 1957.51 :cal AD 1958.08] 0.069 [cal AD 1999.17 :cal AD 1999.41] 0.015 [cal AD 1999.92 :cal AD 2003.10] 0.895 [cal AD 2003.34 :cal AD 2003.80] 0.020

(*) Calibrated with INTCAL13 database (Reimer et al., 2013), both before 1950 and after 1950 using North Hemisphere Zone 2 data (Hua et al., 2013). Preferred age range in bold.

Table 4. Cosmogenic ^{10}Be depth profile data.

Sample Id	Depth [cm]	Thickness [cm]	Dissolved mass [g]	Carrier mass ^a [g]	Corrected for blank ¹⁰ Be/ ⁹ Be	¹⁰ Be concentration [atom/g]	AMS uncertainty	Total ^b uncertainty
EAO0201	250	10	70.6706	1.0155	4.14E-13	1.083E+05	8.5%	9.8%
EAO0202	200	7	53.3308	0.9820	3.60E-13	1.205E+05	2.0%	5.3%
EAO0204	115	5	66.3264	1.0103	7.48E-13	2.074E+05	17.0%	17.7%
EAO0205	95	4	51.4976	0.9890	5.16E-13	1.803E+05	2.0%	5.3%
EAO0206	76	5	49.6240	1.0024	5.23E-13	1.924E+05	2.0%	5.3%
EAO0207	61	5	50.6857	1.0041	5.52E-13	1.991E+05	2.0%	5.3%
EAO0208	46	6	50.4136	0.9783	5.39E-13	1.903E+05	2.0%	5.3%
EAO0209	31	5	50.1676	0.9991	5.30E-13	1.921E+05	2.0%	5.3%
EAO0301	313	14	34.4286	0.9707	1.50E-13	7.681E+04	2.0%	5.3%
EAO0302	254	8	16.8939	0.9843	7.77E-14	8.233E+04	2.0%	5.3%
EAO0303	204	7	41.5267	0.9639	2.04E-13	8.634E+04	2.0%	5.3%
EAO0304	175	7	51.2987	0.9839	2.60E-13	9.081E+04	2.0%	5.3%
EAO0305	149	6	41.4480	0.9832	2.30E-13	9.941E+04	10.0%	11.3%
EAO0306	133	7	41.6932	0.9733	2.42E-13	1.028E+05	2.0%	5.3%
EAO0307	111	7	43.4100	0.9838	4.39E-13	1.810E+05	10.0%	11.3%
EAO0308	95	7	26.3019	0.9929	2.15E-13	1.478E+05	2.0%	5.3%

(a) Mass of Be carrier solution added, at a density of 1.01 g/ml, with Be concentration= 275 micrograms/mililiter.

(b) Used in the modeling input parameters; obtained adding in quadrature 5% uncertainty from reproducibility of Be-10 measurements after chemistry procedures at Dalhousie.

Table 5. Depth profile age model^a results.

Profile Id	Age [ka]	Uncertainty 2-sigma [ka]	Inheritance [10 ⁵ at/g]	Uncertainty 2-sigma [10 ⁵ at/g]	n ^b
EAO-2	37.1	+13 -12	1.087	+0.184 -0.223	1000000
EAO-3	57.6	+19 -17	0.667	+0.116 -0.098	1000000

(a) Depth Profile Model Matlab code (Hidy et al., 2010), version 1.2. Production rate at the sites computed using the CRONUS calculator version 2.2 (Balco et al, 2008). Error in total production rate for model: 20%. Error in half-life of Be-10: 2%. Mean attenuation length for neutrons: 160±5 g/cm².

(b) Number of runs of the model.

Figure 1
[Click here to download high resolution image](#)

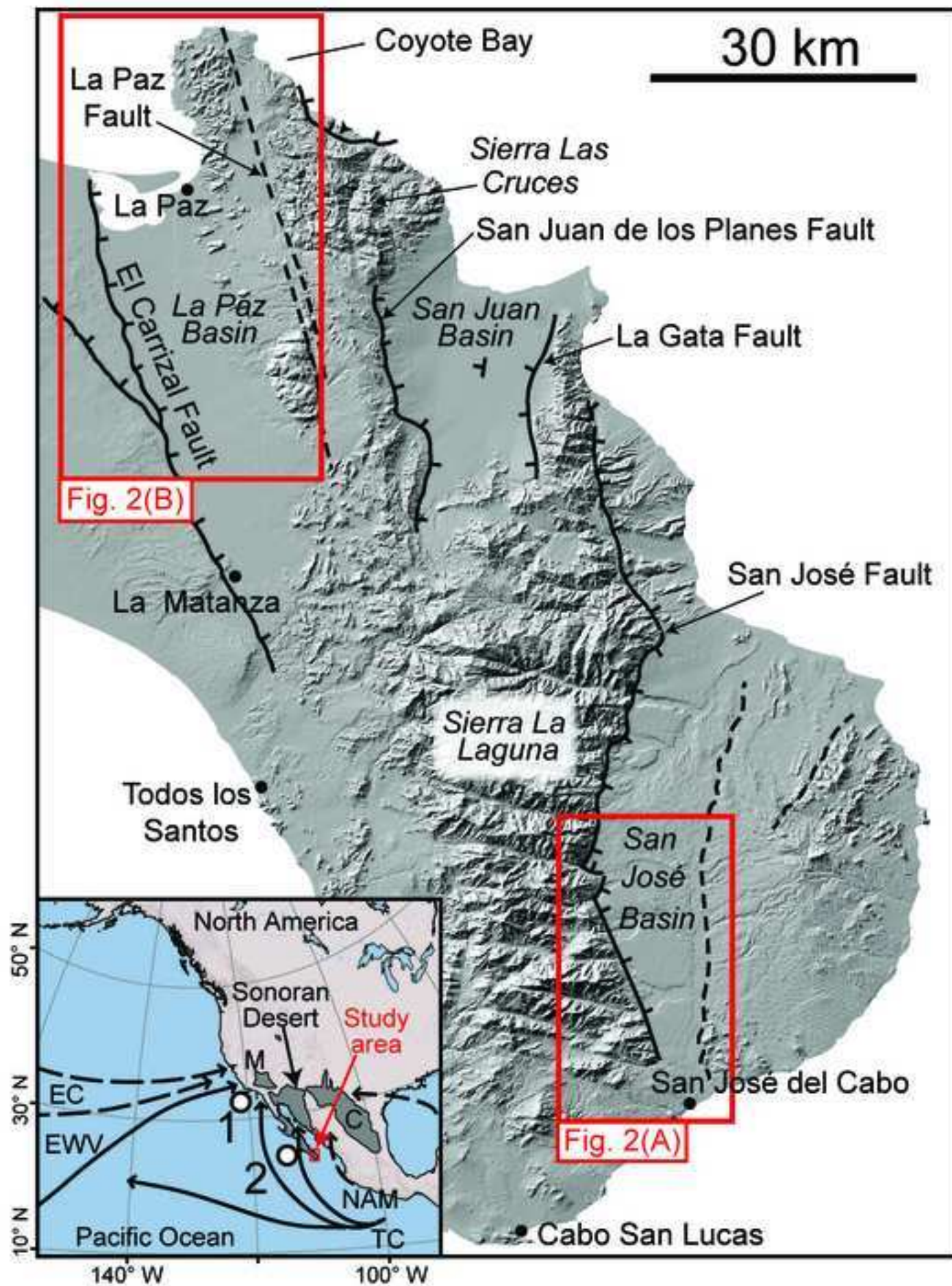


Figure 2
[Click here to download high resolution image](#)

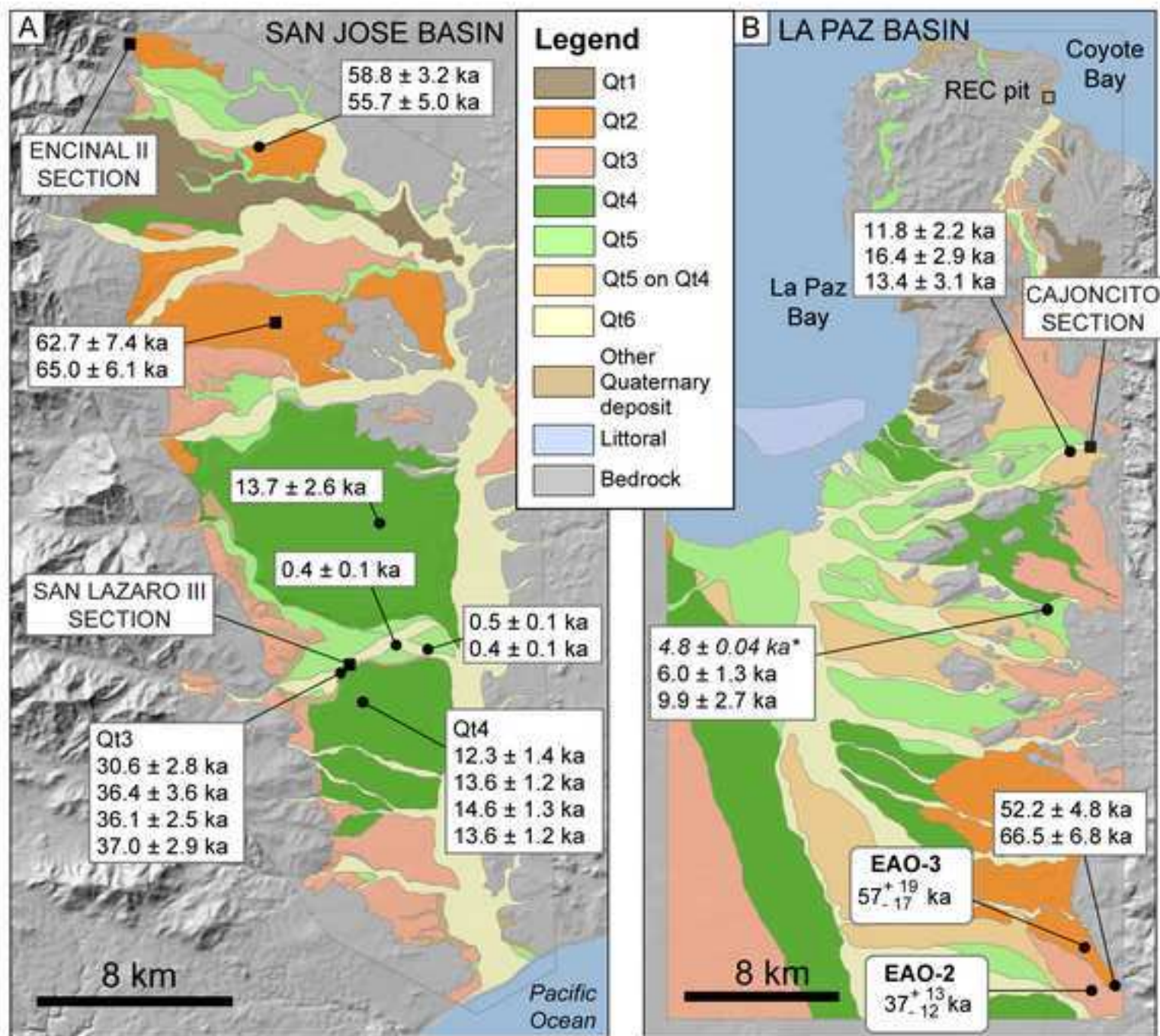


Figure 3
[Click here to download high resolution image](#)

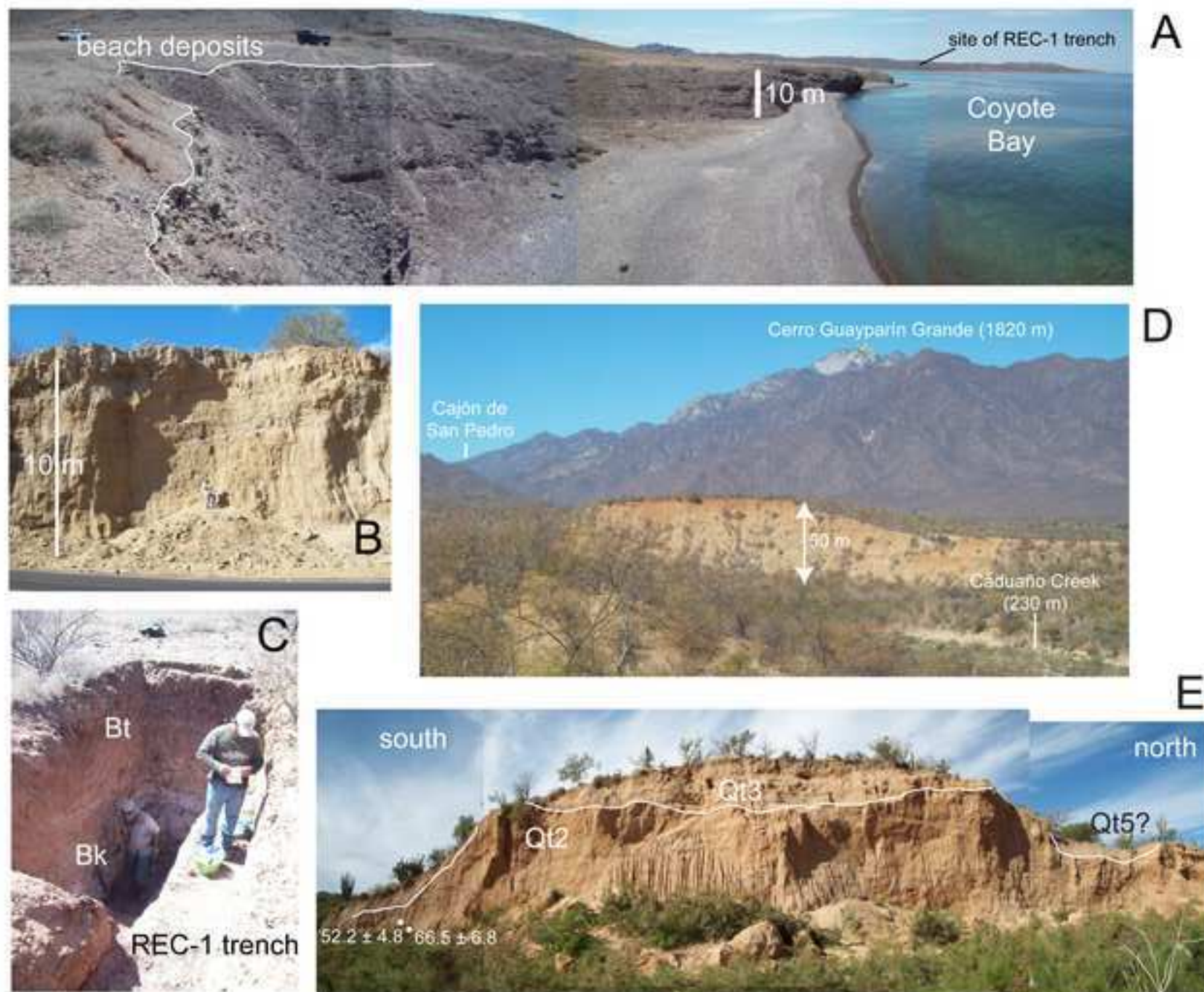


Figure 4
[Click here to download high resolution image](#)

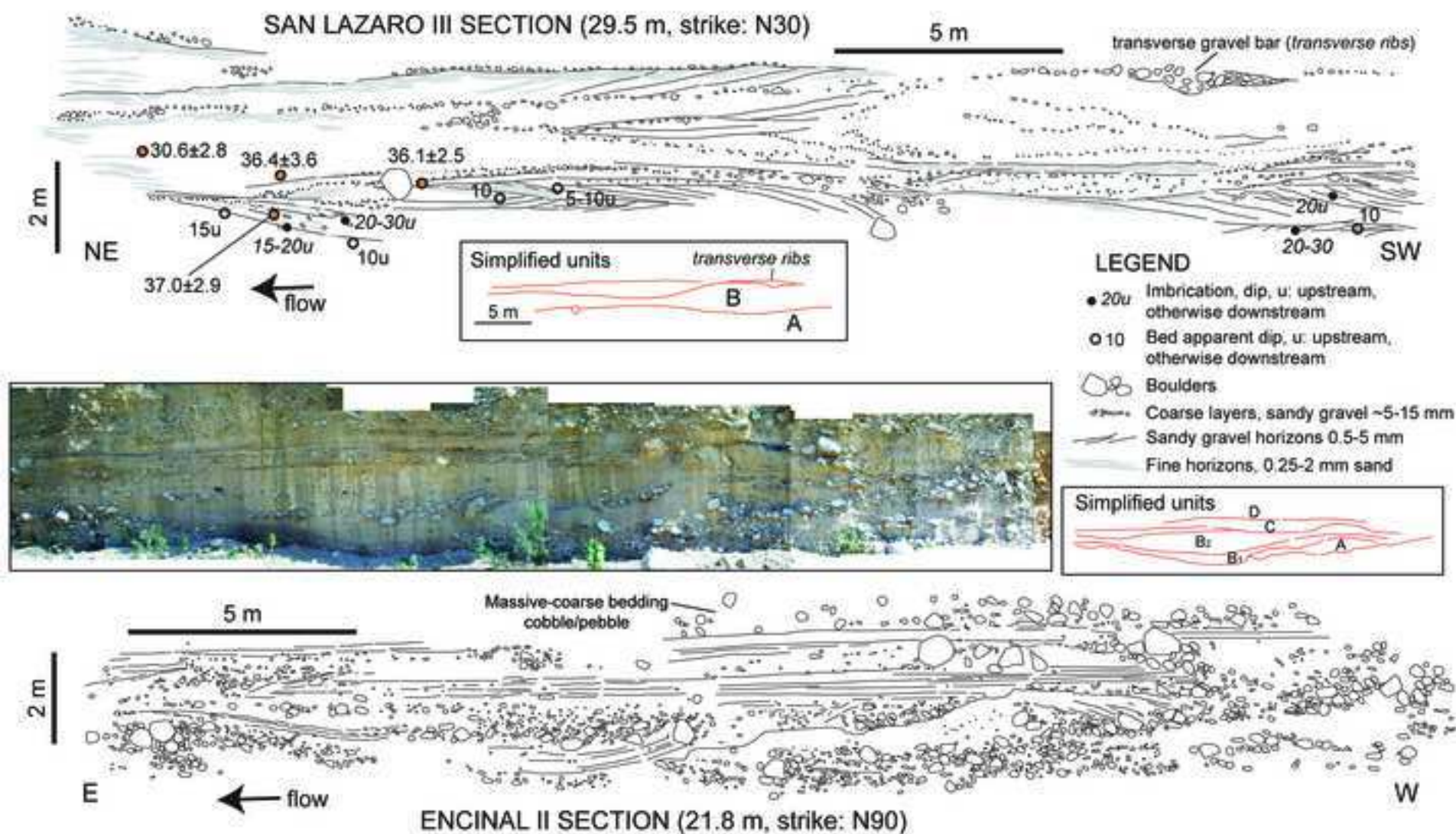


Figure 5
[Click here to download high resolution image](#)

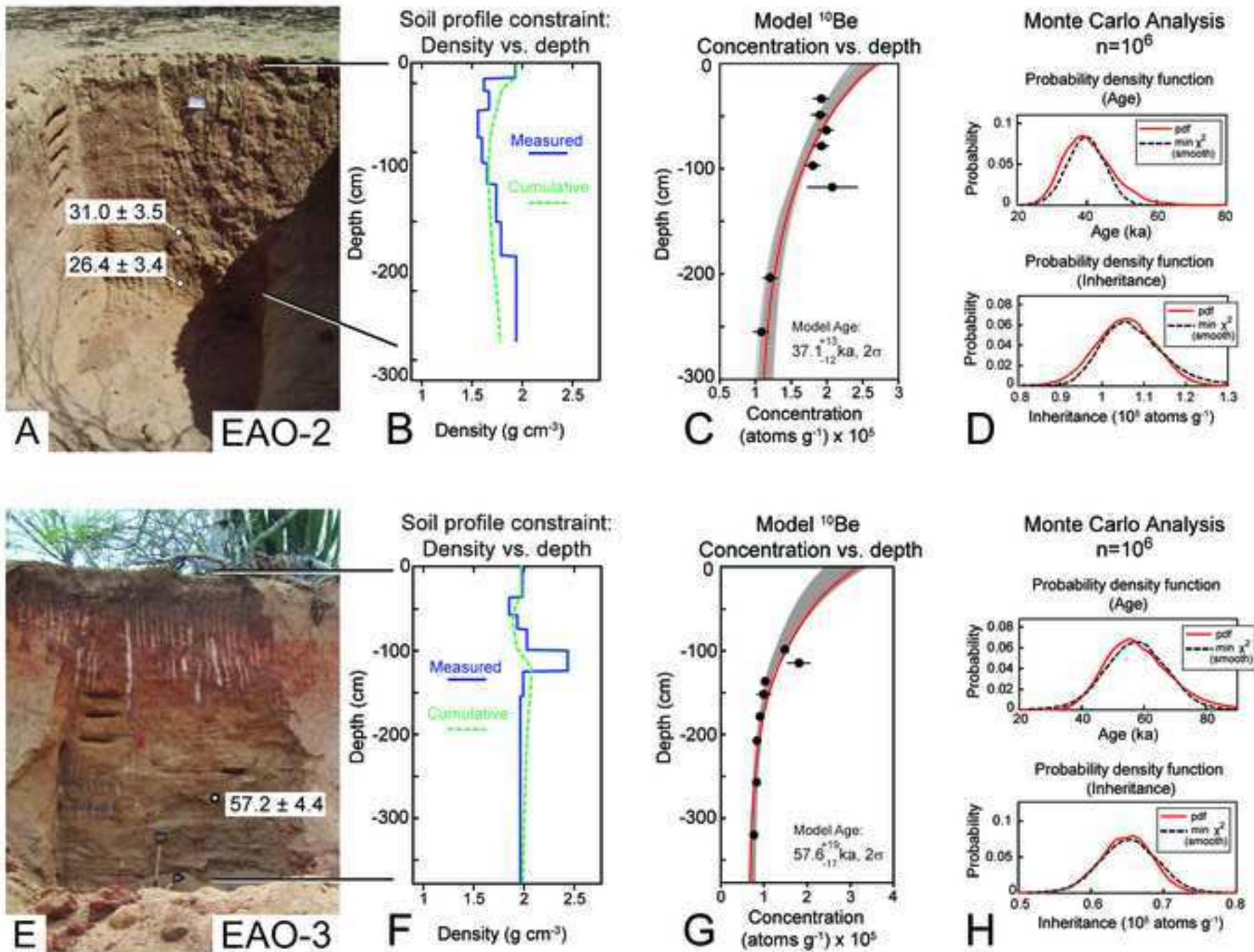


Figure 6
[Click here to download high resolution image](#)

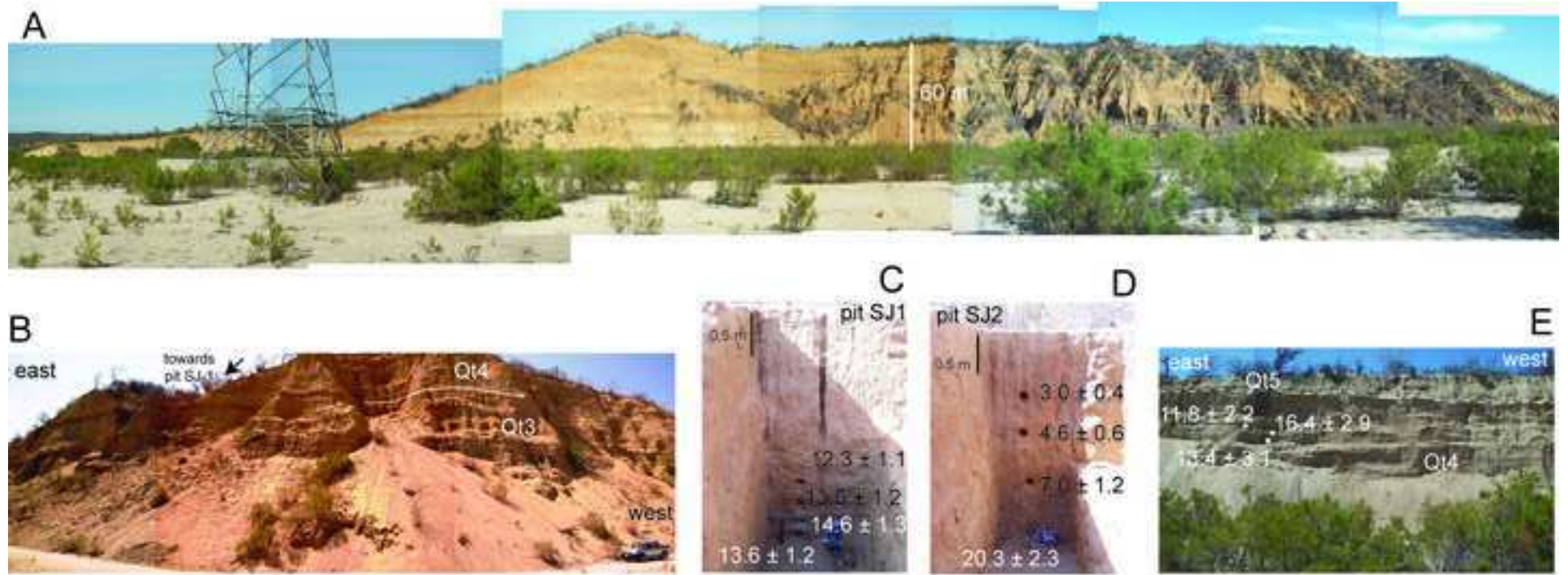


Figure 7
[Click here to download high resolution image](#)

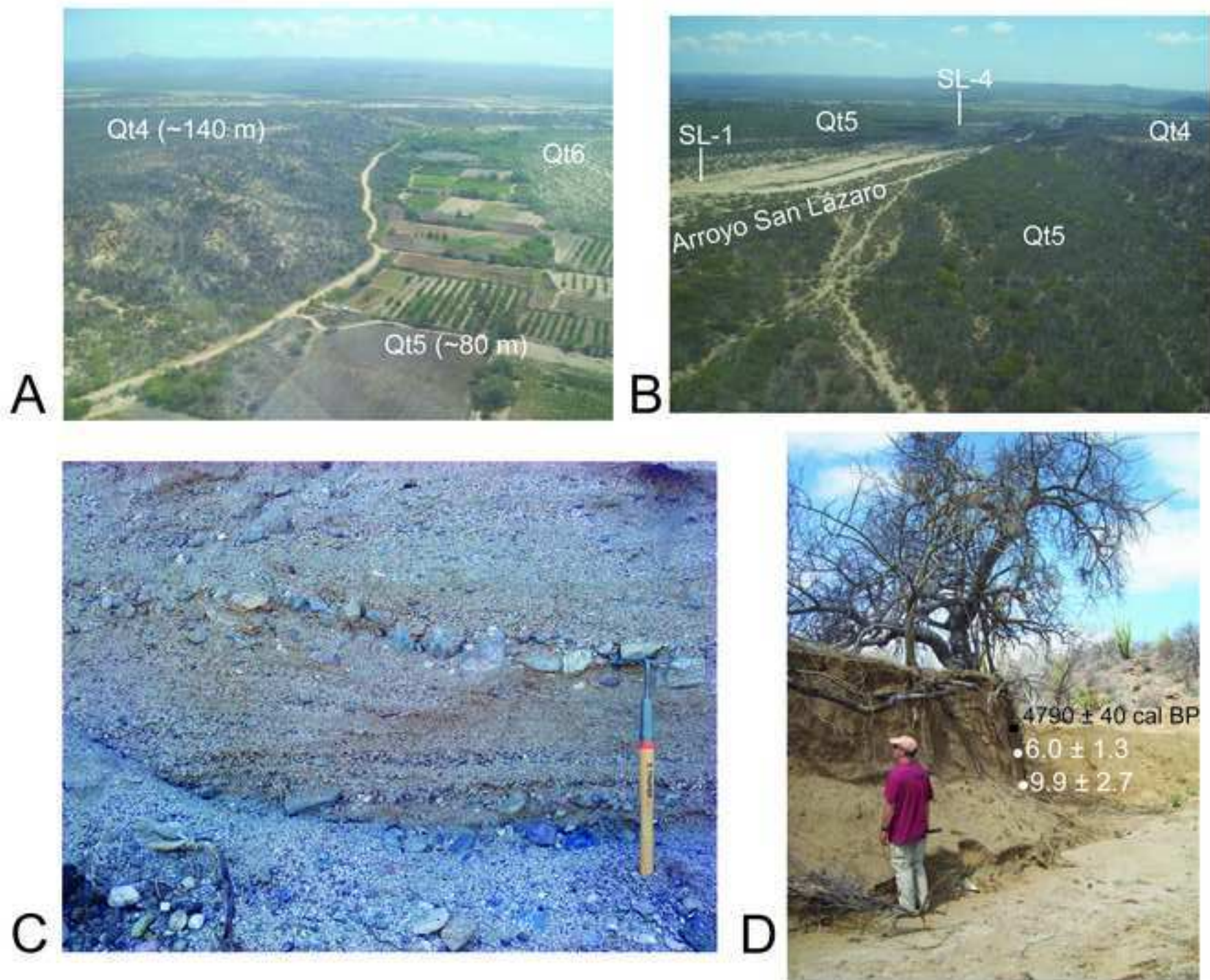


Figure 8
[Click here to download high resolution image](#)

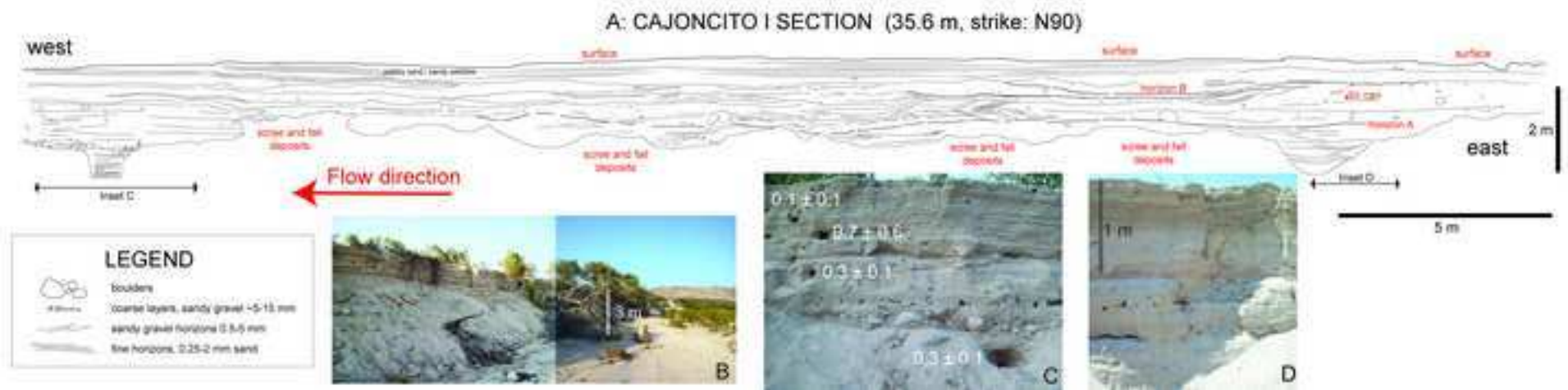


Figure 9

[Click here to download high resolution image](#)

